Paraffin Assisted Graphene Transfer

Master's Thesis, 19.12.2023

Author:

Abhishek Thakur

Supervisor:

Andreas Johansson, Senior Researcher
(Department of Physics)

UNIVERSITY OF JYVÄSKYLÄ
DEPARTMENT OF PHYSICS

Abstract

In this master's thesis, we propose Paraffin support layer as an alternative to the well-established and widely used PMMA for CVD grown Graphene transfer process. The motivation behind the project being to eliminate the two key drawbacks of PMMA transferred graphene. First, the leftover PMMA residue after layer removal, which contaminates and reduces the quality of the final film. Second, the cracks and wrinkles observed in the graphene post-transfer. In the works of Leong et. al. and Villa et. al., they demonstrate that paraffin helps mitigate these issues as it is easier to remove, thanks to its alkane properties and low melting point. Furthermore, paraffin also has a higher coefficient of thermal expansion which can be utilized to stretch the graphene during transfer to help get rid of wrinkles and its flexible nature helps keep the graphene intact.

In our work, we tried recreating those results by simulating similar transfer parameters to the best of our ability as well as trying some different iterations of our own. Our results show some promise in terms of obtaining cleaner and wrinkle free Graphene, but keeping large areas of the films intact during transfer remains a challenge. Thus, further optimizations at several stages of the transfer process are required.

Preface

This master's thesis project was done at the Nanoscience Center and the Department of Physics at the University of Jyväskylä under the supervision of Andreas Johansson, Senior Researcher. The thesis and project were done over the course of summer and fall, 2023. The majority of the lab-work was conducted in the cleanroom located at the Nanoscience Center, while the Atomic Force Microscope Laboratory and the Raman Spectrometer, located in the Laser-lab were used for sample analysis and characterization. Software like the Brukker Nanoscope Analysis, Omnic Raman Map Viewer and Origin were utilized for data processing and image analyses. The majority of the literature research and review for the thesis were done using the Google Scholar and Elsevier Publishing services, in addition to the Mendeley Reference Manager for citing and organizing references.

I would like to express my extreme gratitude towards Andreas Johansson for his supervision and guidance throughout the course of the project and providing his valuable insight along the way. I would also like to thank Olli Rissanen, Laboratory Technician, and part of Andreas' NanoCarbon Group at the Nanoscience Center for providing the high-quality samples throughout the project and helping me learn to operate the Raman Spectrometer. Last but not least, I also want to thank Johannes Parikka, PhD scholar from Jussi Toppari's group, for helping me learn and operate the Atomic Force Microscope.

Jyväskylä, Finland

Abhishek Thakur

Contents

1. Introduction

Graphene, the densely packed singular carbon atom layer, had piqued researchers' interest because of its exceptional crystalline and electronic qualities for well over 60 years before it was successfully isolated by *Novoselov et. al.* in 2004.[1,2] Since then, graphene has found its applications in modern day electronics, sensor technologies, biomedical devices and much more. It would not be too far-fetched at all to say that today, it is one of the most important areas of research in Nanotechnology. But although its benefits remain countless, fabricating ultra-clean large-scale graphene remains a challenge to this day.

Chemical Vapor Deposition (CVD) is the most utilized route for graphene synthesis which involves catalytic growth of graphene on a catalytic metal surface under high pressure and temperatures followed by annealing to induce secondary grain growth. Other methods include Molecular Beam Epitaxy (MBE), some organic synthesis processes or the more primitive mechanical cleavage graphite flakes, or scotch tape exfoliation of Highly Ordered Pyrolytic Graphite (HOPG). Some other lesser prevalent methods include the synthesis of graphene nanoribbons by aerosol pyrolysis.[3,4]

Although CVD remains the most widely preferred method for graphene synthesis due to its ability to produce large scale and high-quality graphene, it mandates a final transfer process from the growth substrate to the target substrate. But due to the extremely fragile nature of graphene, a support layer is usually needed to hold the graphene intact. While other methods like *metal assisted, thermal tape assisted or natural polymer assisted graphene transfer* are used, the most widely employed method uses Poly (methyl methacrylate) (PMMA) as a support layer for cost effectiveness, compatibility with substrates and relative cleanliness of the final films due to its low molecular weight. But the use of any kind of support layer introduces two major issues: the first being film contamination due to the support layer residue. The second issue is film wrinkling due to the thermal expansion coefficient mismatch between the catalytic growth substrate and graphene layer. These wrinkles are then preserved by the PMMA during transfer.[5,6]

In this thesis, we propose Paraffin Wax as an alternative to PMMA assisted graphene transfer in an attempt to rectify the two major shortcomings of the latter, as mentioned above. Paraffin, as opposed to PMMA, does not interact covalently with graphene hence, reducing residual contaminations. Its high thermal coefficient makes it more flexible and expandable,

helping take care of the surface stresses resulting from the rigid nature of the PMMA layer during transfer which would result in a flatter and wrinkle free graphene film, post transfer.[5–7]

2. Graphene: Properties and Background

Graphene is a monolayer of sp^2- hybridized carbon atoms packed in a hexagonal lattice. Each carbon atom has three neighboring atoms bonded through σ-bonds at 120º angles and bond length of 0.142 nm (see Figure 1).[8] Some of its most notable properties that have put graphene on the map for researchers have been its mechanical properties, high electron mobility, thermal conductivity and optical transmittance.[9] thermal conductivity of 5000 W/m.K and a 97.5% optical transmittance.[5]

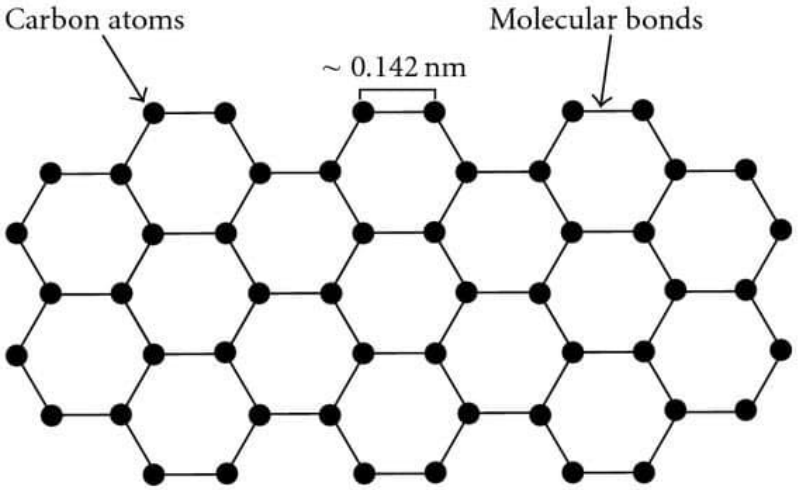

Figure 1 Molecular Structure of Graphene (adapted from Lu et. al. (2012))[8]

When they first successfully isolated single layer graphene films through mechanical exfoliation i.e., repeatedly peeling of pyrolytic graphite in 2004, *Novoselov et. al*. reported that they observed an electron mobility of 10,000 $cm^2 V^{-1}s^{-1}$ at room temperatures for these films that were as large as 15 μm in size.[1,8] Since then, with advances in synthesis methods and the advent of novel and more cost-effective methods like Chemical Vapor Deposition (CVD) growth of graphene. CVD, as opposed to the rather primitive exfoliation, which was both expensive and unsuitable for large scale productions, has brought about cleaner films with ambient electron mobilities as high as 250,000 $cm^2 V^{-1}s^{-1}$.[3,5,10] The origin of graphene's high electrical conductivity can be explained due to its overlap between valence and conduction bands. Since 3 of the 4 outer shell carbon atoms are available for bonding in the

2-D space, the fourth delocalized electron acts as a mobile charge carrier which allows graphene to be highly conductive.

In addition to being highly conductive, graphene also exhibits exceptional mechanical properties with an Elastic Modulus, E ~ 1 TPa and Tensile Strength of up to 130 GPa.[5,9] In their study for the effect of wrinkles in graphene *Min and Aluru* reported the fracture stress for flat graphene films ~97 GPa at ambient temperatures.[11] The thermal conductivity for graphene can be as high at 5000 W/m.K which is almost 5 times higher than it is for graphite.[5] These properties make graphene a solid contender for flexible nano-mechanical and nano-electronic devices such as nano-sensors, conductive films, actuators etc.

Graphene is also hydrophobic in nature and relatively stable at high temperatures, but it tends to show variation in its reactivity when the temperature is varied. Exhibiting spontaneous reduction and oxidation at lower and higher temperatures respectively. Mono-layer graphene films have chemically active edges, making them much more reactive than thicker multilayer graphene. Graphene's reactivity is also greatly affected with introduction of impurities.[12,13]

Pristine graphene on its own, despite its extremely desirable properties, has proved itself to be quite challenging to synthesize, that along with its fragile nature makes it difficult to be incorporated into other aspects of material science, for example, for developing novel polymer nanocomposites. It also shows poor solubility and high agglomeration in solutions.[14,15] To bypass these drawbacks, derivatives like Graphene Oxide (GO) and reduced Graphene Oxide (rGO) have captured researchers' interest. These have found their applications for developing novel polymer nanocomposites. [12,14] GO resembles the same benzene ring structure of pristine graphene, but has additional oxygen based functional groups attached to the surface which serve as activated sites for further chemical reactions (see Figure 2). GO can be subjected to reduction through a number of methods to eliminate most of the excess oxygen groups and sp^3 carbon to generate rGO which is closer in resemblance to pristine graphene. This allows GO and rGO to be used as reinforcement material in nanocomposites.[14,16]

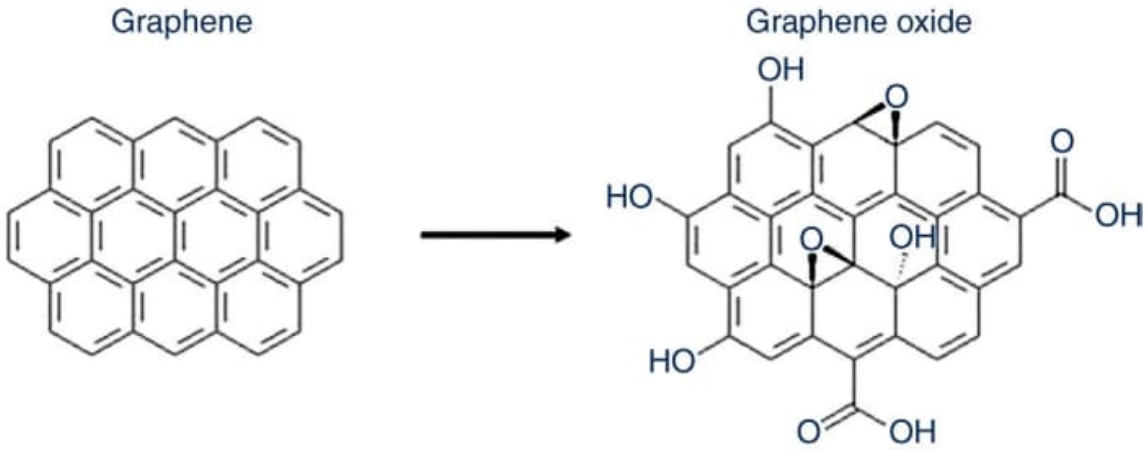

Figure 2 Conversion of Graphene to Graphene Oxide (adapted from Pinto et. al. (2013))[15]

2.1 Graphene Synthesis

As discussed before, the first successful isolation of graphene films was achieved by *Novoselov et. al.* in 2004 by repeatedly peeling off pyrolytic graphene flakes. While successful, this method was not sustainable as it was neither cheap nor suitable for large scale production. [1,8,10] Since *Novoselov et. al. successfully* managed to isolate monolayer graphene films in 2004,[1] the exploded interest in graphene led the researchers across the globe to undertake numerous endeavors to produce graphene at a larger scale for various applications. As a result of those unrelenting efforts, today we have a number of routes for synthesizing graphene. These range the more primitive methods like dry exfoliation of Highly Ordered Pyrolytic Graphite (HOPG) to the more sophisticated methods like Chemical Vapor Deposition (CVD) that are capable of producing large scale graphene layers at a faster rate while keeping the production cost-effective.

Mechanical cleavage of graphite to obtain graphene involves putting a crystalline graphite in an adhesive tape and repeatedly peeling it off until the desired film thickness is obtained. The films or layers are then suspended in a liquid medium or directly transferred on to the target substrate like, borosilicate glass.[1,3,10] This is a more "hit-and-trial" approach and there is no way to predict the yield, or the time taken. The next route for preparing monolayer graphene is via thermal or chemical exfoliation of intercalation compounds like GO or rGO, followed by chemical reduction for improved conductivity. There are several methods to produce Graphene Oxide, like the *Hummers Method*, which involves oxidizing graphite in H_2SO_4, $NaNO_3$ and $KMnO_4$. The excess $KMnO_4$ is removed by reducing it to $MnSO_4$, and finally a methanol bath. [3,17] The resultant GO is then thermally exfoliated by rapid heating it to 1050

ºC followed up with spray drying it with 300 ºC air to give monolayer graphene with an approximate 80% yield.[18] But the problem with the methods mentioned above still remains, the inefficiency to produce Graphene at a larger scale for use outside of just lab experiments.

The first use of *Chemical Vapor Deposition* (CVD) for graphene synthesis dates back to 2008 and 2009, where large scale graphene was grown on Nickel (Ni) and Copper (Cu) substrates in high temperature chambers followed by controlled cooling to show the effect of cooling rates on the yield.[19,20] This involved vapor deposition from a hydrocarbon gas on the Ni substrate at 1000 ºC. Next, controlled cooling precipitated large amounts of Carbon from the decomposed hydrocarbon in the substrate's interstitial sites, depending on the solubility of carbon (1.1% for Ni). The diffused carbon then proceeds to segregate at the substrate surface, forming graphene films. For metals with low carbon solubility like Cu, the surface adsorbed carbon atoms become sites of nucleation and grow into graphene layers via secondary grain growth by annealing. The low solubility of carbon atoms in Cu (0.03%) makes it easier to control the number of layers of graphene grown, giving a higher yield of monolayer graphene films.[3,20,21] The Cu films are subjected to annealing to produce grains ranging from 10 μm to 100 μm, but it can also cause the film to break and form de-wetting spots which is usually countered by the grain growth itself when the annealing is done at temperatures closer to the melting point for Cu.[4] Annealing the Cu grown graphene films and controlled cooldown also helps eliminate any leftover residue from reagents, or carbon deposits.

On a polycrystalline Ni substrate, large area graphene films have been reported to consist of anywhere between 1 to 12 layers. Their properties were closer in comparison to the graphene obtained by via mechanical cleaving.[3] The Ni grown graphene films were also very flexible and could be transferred onto flexible polymer substrates like Poly-(ethylene terephthalate) (PET) with roll-to-roll transfer.[3,9] Some other commonly used insulating substrates include Sapphire, SiO_2 and Si_3N_4. Graphene has been grown on Cu (111) at temperatures up to 1000 ºC by CVD of Methane (CH_4) mixed with Hydrogen (H_2) or other inert gases like Argon (Ar), giving a 95% yield of monolayer graphene. However, the monolayer graphene grown on Cu films posed a high risk of structural defects and warranted the use of a polymer support layer like PMMA, in order to relieve the transferred graphene of mechanical stresses.[3,6,20] More will be discussed about the use of support layers for graphene transfer in *Section 3*.

While CVD is the most popular solution for growing large area graphene, devices that utilize these films suffer from various setbacks like low mobilities, impurities etc. Molecular Beam Epitaxy (MBE) is another method that can be employed to synthesize monolayer graphene at a large scale and help bypass these drawbacks[22,23]. The procedure is reproducible and gives thickness control down to the atomic level. Park et. al. (2010) grew graphene by carbon MBE on chemical mechanical polished on-axis 4H-SiC (0001) substrates. They heated the substrate to temperatures as high as 1600 ºC and used fullerene (C_{60}) for the carbon flux source.[23] Another example of the use of MBE was demonstrated by Garcia et. al. (2012) where they synthesized graphene on hexagonal boron nitride (h-BN) at a temperature of 930 ºC. Here, the hexagonal lattice for h-BN lead to an extremely flat graphene layer.[22]

3. Support Layers for Assisted Graphene Transfer

Transferring CVD synthesized graphene on catalytic substrates like Ni and Cu[19,20] to the final substrate can be done with or without a support layer. But as briefly mentioned in Section 2.1, it can induce mechanical stresses due to topological defects like dislocations. Moreover, weak interlayer Van der Waals interactions result in low strength and shear modulus despite the same values being considerably higher in-plane.[24]

The above-mentioned problems necessitate the use of an external support layer that can alleviate the stresses on the graphene during transfer. An early instance of assisted graphene transfer can be spotted in Yu et. al.'s (2010) work, where they transferred graphene grown on Ni surfaces onto insulating surfaces with the use of solidified Si rubber.[19] The metallic substrates can easily be etched away from beneath the support layer coated graphene. Hence, a suitable support layer needs to be flexible, have strong adhesion to graphene, provide mechanical support and should be easily removable after transferring on to the target substrate is completed. The transfer can be assisted with the help of a polymeric layer, a metallic layer or it can also be molecule assisted where the layer is replaced by small molecular carriers like naphthalene[25] which can then be easily removed by sublimation at room temperature.[6]

Polymer based support layers are the most prevalently used nowadays for assisted transfer processes because they fulfil the requirements for an ideal support layer for the most part. They are flexible and therefore ensure proper contact with the graphene, preserve the integrity of the film during transfer by relieving the film of induced mechanical stresses and

can also be easily removed with the help of solvents post-transfer. In addition, these polymer support layers can also withstand an additional step of baking at temperatures upwards on 100 ºC which helps remove moisture trapped between the graphene and target substrate, ensuring proper contact between the two. [6,26] Some of the most widely used polymer support layers include Poly(methyl methacrylate) (PMMA)[27], Polydimethylsiloxane (PDMS)[28] and natural polymers like cellulose acetate[29].

3.1 PMMA Assisted Graphene Transfer

The utilization of PMMA assisted CVD grown graphene transfer can be traced back to 2009 when it was used to transfer graphene grown on Cu foils to SiO_2/Si substrate for high performance electronics applications like Field Effect Transistors (FET).[27] PMMA (see Figure 3 for structure [7]) is a lightweight, non-degradable polymer that has found plenty of applications in biology. Its major component is the methyl methacrylate (MMA) monomer. PMMA has a melting point of 160 ºC and boils at 200 ºC, compressive strengths can range between 85 to 110 MPa and tensile strengths from 30 to 50 MPa. It has a high thermal expansion coefficient between 5 to 10*10−5 $°C^{-1}$, specific heat capacity of 1.7 J/g ºC and also has desirable optical properties.[30,31]

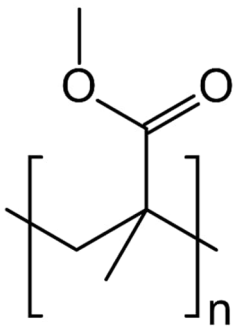

Figure 3 Molecular Structure of PMMA dimer (Adapted from Leong et. al. (2019))[7]

One of the factors that needs to be considered when choosing a support layer is how strong the adhesion forces between the graphene and the support layer are, which ultimately depends on the surface energy of the layer (polymer in this case). The weaker the adhesion, the easier it will be to remove the layer after the transfer and the less residue it will leave behind, ultimately resulting in cleaner, high-performance graphene. [5,6,27] PMMA has sufficiently low

surface energies that makes it suitable for transfer and it can also easily be removed by dissolution in acetone.

The common steps for PMMA based graphene transfer involve spinning a PMMA/Anisole solution on Graphene grown on Cu film at about 2500 rpm. Followed by baking the PMMA/Graphene/Cu sandwich, which removes the PMMA solvent and also initiates cross-linking in the PMMA layer resulting in its polymerization. In the next steps, the Cu film is etched away using suitable etchants like iron-nitrate, or iron-chloride etc. The resultant PMMA/Graphene stack is washed in deionized water before it is scooped up with the target substrate. The PMMA/Graphene/Substrate stack can then be baked to help remove any leftover moisture between the graphene and substrate. Finally, the PMMA layer is dissolved in acetone.[26,27] A schematic for the process can be seen in Figure 4, adapted from Barin et. al. (2014), where they also demonstrate the addition of a second PMMA layer on top of the existing PMMA layer to improve the quality of transferred graphene.[26]

PMMA has several other advantages that make it not only just a preferable support layer but also a widely used polymer for general applications. It is water and weather resistant, immune to organic, inorganic solvents and reagents, some weak acids/alkalis. It is cheap, easily available, transparent so it is used in appliances like lamps, as mobile screens or lens protection coatings.[32]

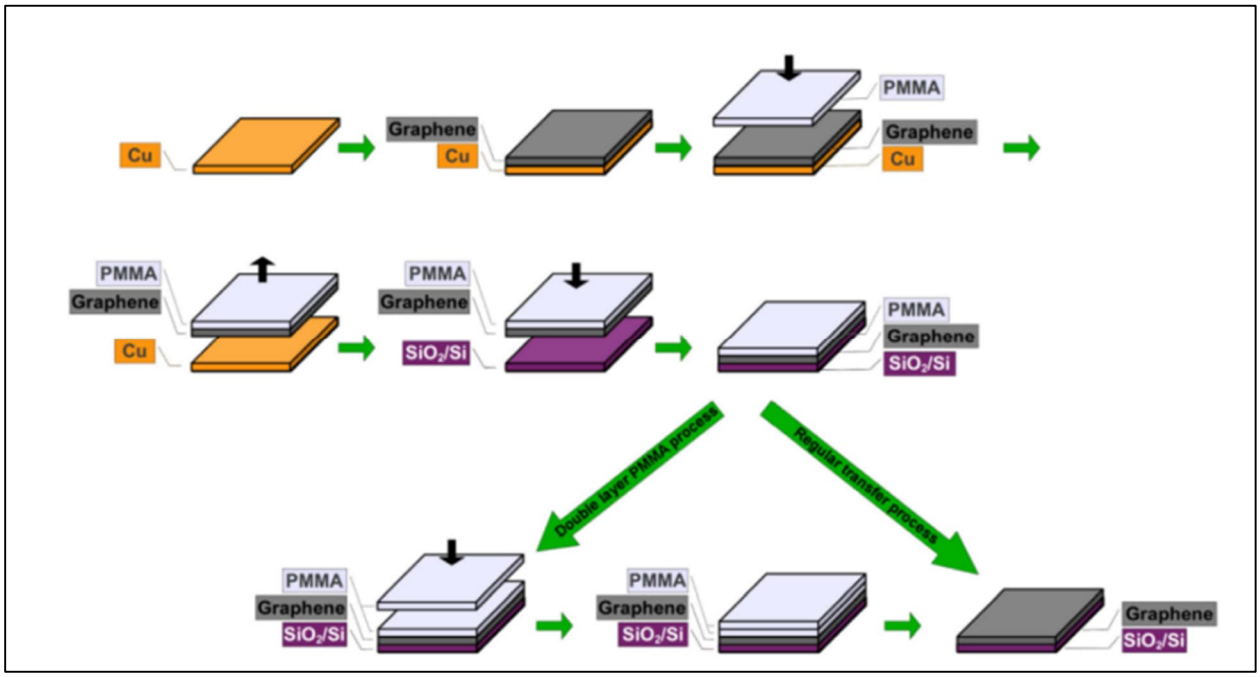

Figure 4 *PMMA Assisted Graphene Transfer Schematic (Adapted from Barin et. al. (2014))*[26]

3.1.1 Drawbacks of PMMA as a Support Layer

Despite its numerous advantages as a support layer, PMMA is not without its flaws. The first and most notable one is the residue that it leaves behind on the graphene layer after dissolution. This occurs due to the covalent interactions that occur between PMMA's functional groups, and the lattice defects present in the graphene (from the CVD).[5,7] Measures can be taken to minimize the residue, like incorporating a final annealing step in the process but some residue is still left behind. The residue has major effect on the carrier mobility of graphene. It can induce doping and, as a result, carrier scattering[26], which makes it difficult to use them in high performance electronics.

Another major issue is the presence of wrinkles and cracks that can occur due to the thermal coefficient mismatch between graphene and the substrates like the Cu film it is grown on. The wrinkles occur when the graphene layer contracts at a different rate than the substrate during the cooldown phase, post-synthesis. The wrinkles are then further preserved during the transfer process by the PMMA layer. These prevent the graphene from lying completely flat with the substrate during transfer. The gaps can affect the forces of adhesion between PMMA-Graphene and Graphene-substrate (the latter needs to be higher) which results in wrinkles and tears when the PMMA is removed.[5,26,27] Several iterations of the PMMA enabled transfer processes have been proposed through the years by scholars to help eliminate these issues. Like the addition of an extra layer of PMMA proposed by Li et. al. which improved the contact between the graphene by mechanically relaxing the first PMMA layer and substrate [27] resulting in low crack densities; or the use of low molecular weight PMMA to further minimize the PMMA residue post-removal, proposed by Kim et. al.[33]

3.2 Paraffin Assisted Graphene Transfer

As discussed in the previous sections, the use of PMMA as a support layer, although the most widespread among researcher for producing large scale monolayer graphene films due to its several advantages has two major drawbacks that result in low quality graphene films. First, the inability to completely remove PMMA residue after the transfer onto the target substrate, which severely deteriorates the carrier mobility of the film. Then there's the presence of tears and wrinkles in the final graphene film.[5,7,33]

To counter these problems, the need for alternate support layers is eminent. Researchers have tried replacing PMMA with alternative polymers like PDMS[28], or natural polymers like

cellulose acetate[29]. Non-polymer-based methods include metal assisted transfers, organic small molecule assisted transfers like the use of naphthalene and utilizing its sublimation properties at room temperatures.[25] Another such novel alternative proposed by Leong et. al. (2019) is the use of paraffin as a support layer for CVD grown graphene.

Paraffin or commonly known as Paraffin Wax is a petroleum derived colorless, odorless polymer with melting points usually somewhere between 40 – 60 ºC, boiling point at 370 ºC, density of 900 kg-m^3 and heat capacity ranging between 2.14 to 2.9 J/g ºC. Its structure (see Figure 5 [7]) consists of straight chain hydrocarbons ranging from C_{20} to C_{30}, with *Hentriacontane* (*$(CH_3(CH_2)_{29}CH_3)$*) being its major component. Although insoluble in water due to its non-polar nature, it is easily soluble in esters, ethers and benzene. Paraffin is combustible but chemically resistant to most reagents and is also an insulator. [34]

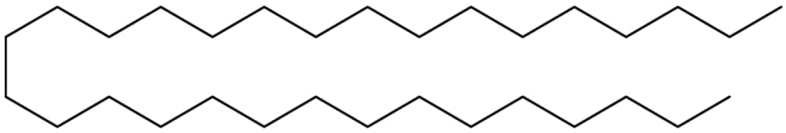

Figure 5 Molecular Structure of Paraffin Wax dimer (Adapted from Leong et. al. (2019))[7]

The interest in paraffin arises from its alkaline nature, which makes it unreactive and avoids the covalent interactions (due to the lack of C = O group present in PMMA) with graphene that could result in contamination of the film, as observed with PMMA. Consequently, paraffin leaves behind much less residue post-dissolution in comparison. It also possesses a higher thermal expansion coefficient which results in the thermal release of the film at temperatures as low as 50 ºC. Moreover, the flexibility and high expansion coefficient can be utilized to stretch out the graphene during the final transfer step which ensures better contact with the substrate, eliminating cavities that could trap moisture and crack the film.[5,7]

Typical paraffin assisted graphene transfer includes spinning molten paraffin on top of a CVD grown graphene layer on a metallic substrate (Cu or Ni films, typically) followed by etching away the metallic films in an etchant like Ammonium Persulphate (APS).[5] The paraffin-graphene stack is then rinsed in deionized water and then scooped up with the target substrate like Si/SiO_2. The next step is baking the stack at temperatures of 40 ºC or lower to avoid melting away the paraffin film and rid any residual moisture from underneath the

graphene. Finally, the paraffin is then removed by dissolution in an organic solvent like hexane.[5,7]

4. Characterization Methods

In this thesis, we utilized two major characterization methods: *Raman Spectroscopy* and *Atomic Force Microscopy*, to compare and determine the quality of the obtained graphene films from the two transfer methods (PMMA assisted, and Paraffin assisted). The analysis was mainly focused on determining the presence of contaminants on the film surfaces and any physical defects like wrinkles, cracks, tears etc., that may have occurred during the processes.

4.1 Raman Spectroscopy

The *Raman Effect* is named after its namesake and discoverer, Sir C. V. Raman from India. He was the first to observe the phenomenon of inelastic scattering of electromagnetic waves off matter when irradiated with light in 1928. Matter, when irradiated with incident light, may scatter some photons that are of a different frequency than that of the incident light. Raman Spectroscopy is the measurement of these shifts in frequency that can be correlated to the nature of the material and used to determine its chemical properties.[35]

When the sample molecules are irradiated, the resulting vibrations put them in a state of induced dipole moments and the scattered electromagnetic waves can enter a virtual energy state. As the molecules eventually return to their ground state, for inelastic scattering this ground state can either shift to higher or lower vibrational energy states. Depending on the direction of this shift, the scattering is either dubbed Stokes or Anti- Stokes scattering. Stokes scattering occurs for a shift to a higher energy state where the emitted photon will have lower energy than the incident photon. On the other hand, Anti- Stokes scattering occurs if the shift is to a lower energy state where the emitted photon will possess higher energy compared to the incident photon.[35,36]

The instrumentation for Raman spectroscopy is also rather simplistic in contrast to other vibrational analysis techniques like Infra-Red (IR) spectroscopy that require sample preparation which can potentially contaminate the sample and involve complex signal preparation and processing. On the other hand, all Raman spectroscopy virtually requires is sample excitation by irradiating it with a strong beam of light, which has been severely

simplified ever since the advent of laser sources, and to collect the scattered light with a spectrometer.[35]

Raman Spectroscopy has played a fundamental role in biological analysis because water gives off very weak Raman signals, making it easier to analyze things of interest. Its ability to analyze live samples is also another big advantage that it holds for biologists.[35] (Nano-) Material scientists have also been extensively taking advantage of Raman spectroscopy for several decades now. It is a powerful and versatile characterization method that is popular due to its plethora of use cases. It offers a fast, high-resolution, non-destructive means of analysis and avoids the need for any kind of physical changes to the sample like compression, dissolving in a liquid medium etc. This is especially of high-value when working with extremely fragile, atomically thin films like graphene.[35,37] The Raman data offers a large data pool with many prominent features in the spectra like peak positions, intensity and Full Width Half Max (FWHM). These can be extremely helpful in analyzing things like chemical and electrical properties of the material, detect the presence and nature of impurities on a sample surface, phonon frequencies and much more.[36]

4.1.1 Raman Spectra for Graphene

The Raman Spectra for graphene (see Figure 6 [38]) consists of distinct peaks or bands, among those G, D and 2D bands are the most prominent ones, that are interpreted to obtain relevant information about the films (Figure 3).[36,37] The G-band, which is usually observed at about 1580 cm^{-1} for monolayer graphene, is a result of the two doubly degenerate phonon modes, Longitudinal Optical (LO) and in-plane transverse optical (iTO); out of its six normal modes in the Brillouin Zone (BZ) center.[37] It represents the high frequency E_{2g} phonon.

The G-band's intensity and position can be used to directly predict the nature (single, double, triple layer) of the graphene. The intensity shift with the number of graphene layers present is almost linear as a higher G-band intensity correlates to multiple layers. Also, the position of the band shifts in relation to the number of layers. As the number of layers increases, the band shifts to a lower wavenumber on the spectrum.[39]

The D-band, usually observed at about 1350 cm^{-1}, is the result of the six-atom rings' breathing modes. It is disorder activated and activates when the rings' π- orbitals interact.[37] Therefore, the D-band peaks give information about contaminations present in single layer graphene or presence of multiple layers of graphene such as in graphite. It can also be used to

observe the degree of chemical modification of graphene.[39] The 2D (also known as G') band which is observed at about 2700 cm^{-1} in the second order spectra, activates due to two phonon lattice vibrations whereas the D-band occurred due to one phonon lattice vibrations and hence, does not need any defects or contaminants to be activated.[37,38]

The 2D-band's shape can be used to determine the number of layers present in the graphene film. It's more symmetrical, with a Full Width Half Max (FWHM) at 30 cm^{-1} and the symmetry lowers as the number of layers increase. Both the D and 2D band frequencies change as a function of the incident laser energy with the slope of 2D-band being double the slope of the D-band. The intensity ratios for the 2D and G-band is also used to determine the nature of the films as the typical intensity ratio (I_{2D}/I_G) is greater than or equal to 2 for monolayer graphene.[39] Another weak band that is also disorder induced, is the D' band occurs at around 1620 cm^{-1}.[38]

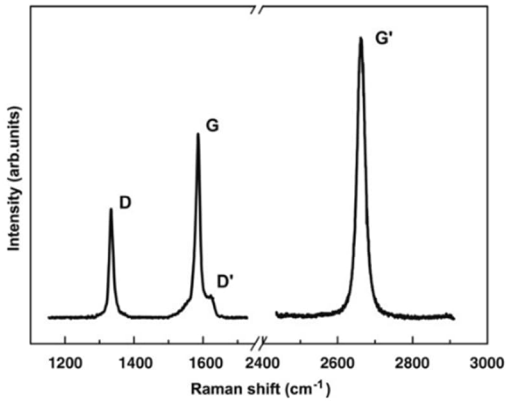

Figure 6 Raman Spectra taken on the edge of a single layer graphene (adapted from L.M. Malard et. al. (2009))[38]

4.2 Atomic Force Microscopy (AFM)

Atomic Force Microscope (AFM) is a high resolution and sophisticated piece of technology whose advent in 1986 (developed by *G. Binning, C.F. Quate & H. Rohrer*) revolutionized and simplified the area of surface imaging and characterization in all fields ranging from medicine to materials science.[40] Commercial AFM's can measure details on a surface down to its atomic configuration. Some of the many advantages that AFM holds over other microscopy techniques include its flexibility of sample environment that allows it to image samples at room temperatures, in air etc. There is also no need to coat the sample surfaces to make them conductive like in case of Scanning Electron Microscope (SEM). A variety of samples like, ceramics, glass, polymers, highly viscous samples or liquids can be analyzed.[41]

It is also non-destructive to the samples which makes it suitable for imaging delicate samples like Graphene as used for the purpose of this thesis. It is fast, gives the user refined control and clear images. Moreover, it can also be used to analyze surface forces in different scanning modes and obtain a 3-D topographical map of the sample surfaces.[40]

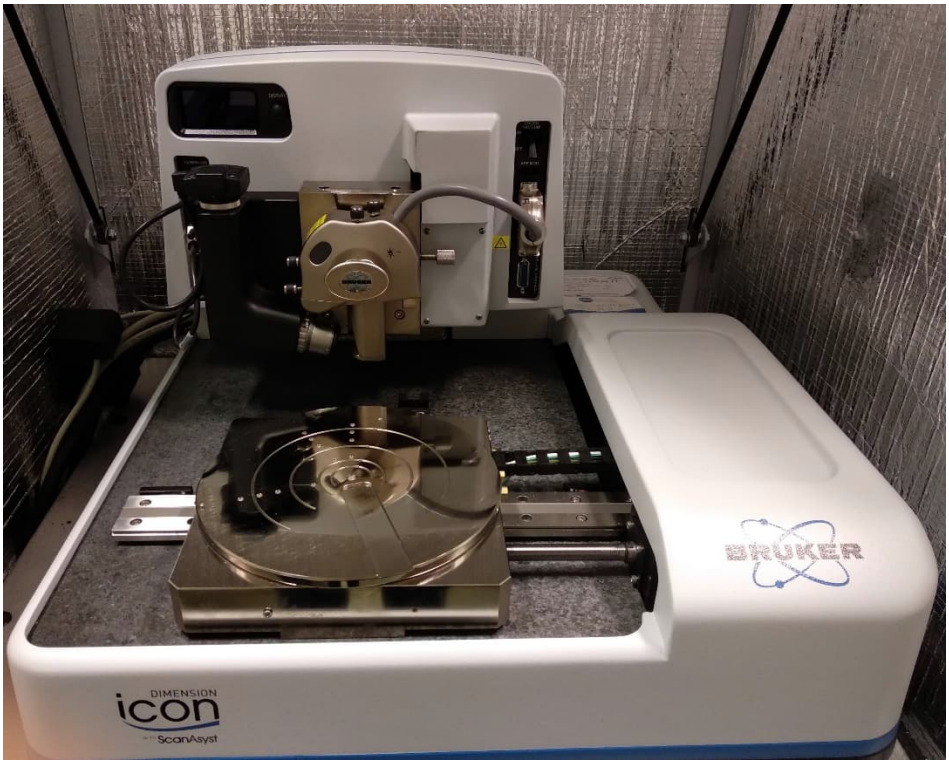

Figure 7 *Bruker Dimension icon ScanAsyst AFM at the NanoScience Center (JYU)*

The key underlying working principle of an AFM is the interatomic interactions between the atomically sharp tip and the atoms present on the surface being scanned. The basic components that comprise an AFM are, a nanoscale tip, diameter 4-24 nm (for our measurements), attached to a cantilever, a photodiode, a photo detector and piezo-electric translators.[41] As the tip scans along the surface, it moves in response to its topography and Van der Waals forces exerted between the tip and the sample. The up and down motion of the tip bends the cantilever, off which a laser beam is reflected towards a photodetector. The change in the detector signal due to the bending of the lever is correlated to the surface profile and a map (or image) is generated. The signal is also passed through a feedback loop that consists of proportional, integral, derivative or PID controllers which optimize scanning speed, setpoints etc.[40,41]

Another major component of the AFM setup are the piezoelectric translators. These transducers expand or contract in response to applied electric potential. Typical expansion

coefficients are as low as 0.1 nm/V, giving extreme precision to measurements. The feedback from the cantilever twist, which in turn changes the laser position, is used to vary the voltage through the transducer to adjust the force applied to the surface on the fly, giving extremely precise topographical data.[40]

The AFM has a wide range of use cases; hence, it can be operated in several modes depending on the needs of the user. For topographical measurements, there are two main modes, namely, *contact mode* and *oscillating mode*. *Contact mode* is the most straightforward of the two. The probe tip is in constant contact with the sample surface. As it drags along, any variations on the surface deflect the cantilever which changes the laser position, which in turn causes variation in the photodetector signal. This is then translated to generate topographical data about the surface. The major drawback of this mode is the quick tip wear, shear forces in the scanned surface and surface damage.[40]

In the *oscillating (non-contact) mode*, the tip is oscillated above the surface and the variations in the phase and amplitude of the oscillations as it approaches the surface due to the atomic forces is used as the feedback signal to give more accurate data. The surface can be scanned such that the probe never comes in contact with the sample surface, and only the long-range atomic forces come into play. There can also be a *tapping mode* where the tip comes in intermittent contact with the surface. The oscillating mode is the most widely used mode for imaging all sorts of samples, even liquids. The intermittent contact or tapping mode can be used to measure material properties like the viscoelasticity of liquids.[40,41]

Other non-topographic modes are also employed for specific use cases. For example, the mechanical property mode, which is used to measure mechanical properties like stiffness, viscoelasticity, usually utilizes *phase imaging* the sample in response to amplitude variations in the tip oscillations. *Adhesion forces* also come into play here that dampen the oscillations and cause amplitude variations. Vertical surface interactions like adhesion and pull off heights are then utilized to conduct *force spectroscopy*. *The Nanoindentation* mode is another contact mode for AFM which can be utilized to approximate more mechanical parameters like Young's modulus and spring constants of the material.[40,41]

There is also the possibility to conduct Lateral Force Microscopy (LFM) which records the lateral bending of the cantilever as the tip scans the surface. The slope of this variation gives information about lateral forces or friction along the surface but it's hard to distinguish whether the variations are due to topographical defects or actual frictional forces hence, the

sample surface would need to be extremely flat. LFM is complex to utilize because it requires additional complex equipment and it's a relatively less used mode.[40]

5. Methodology

The experimental phase for this work mainly involved three steps, synthesizing graphene on Cu films that were initially grown on Sapphire substrates using the methods described by Miller et. al. (2013)[4]. Next, transferring the synthesized graphene onto target substrates (SiO_2) using PMMA and Paraffin as support layers followed by characterization of final transferred films using the two methods. The following sections discuss the synthesis and transfer processes in detail.

5.1 Graphene Synthesis at the Nanoscience Center, JYU

The graphene growth process utilized here is an adaptation of the work described by *Miller et. al. (2013).*[4] They demonstrated that it was possible to transform Cu films deposited on α-Al_2O_3 (0001) into large grain Cu (111) via subsequent annealing. Cu (111) is suitable for CVD growth of graphene due to their similar hexagonal lattice structures with a lattice mismatch as low as 3.8%. This makes Cu (111) suitable for graphene growth as it can almost be seen as a template for its lattice, and it induces less strain and rotational disorders in the films.[4]

We start by cutting down a Sapphire wafer which is typically 430 µm thick, into 5 mm x 5 mm pieces using a circular saw. The pieces are then cleaned in 3 stages. First, via sonication in a hot acetone bath for 20 minutes followed by another 20 minutes sonication in a 1:1 IPA:H_2O mixture. Finally, a 20-minute sonication in acetone followed by rinsing with IPA. The cleaned Sapphire pieces are then annealed in an O_2 atmosphere in the *Carbolite CTF 12/65/55* Alumina tube furnace for 12 hours followed by a cooling period of 6 – 8 hours.

We then evaporate crystalline Cu on the Sapphire chips using the *Balzers Baltec BAE 250* vacuum e-beam evaporator (Figure 8). 12 annealed Sapphire pieces are placed on the sample holder and an approximately 400 nm thick Cu film is evaporated onto them at a rate of 5 Å/s under a vacuum pressure $< 5 \times 10^{-5}$.

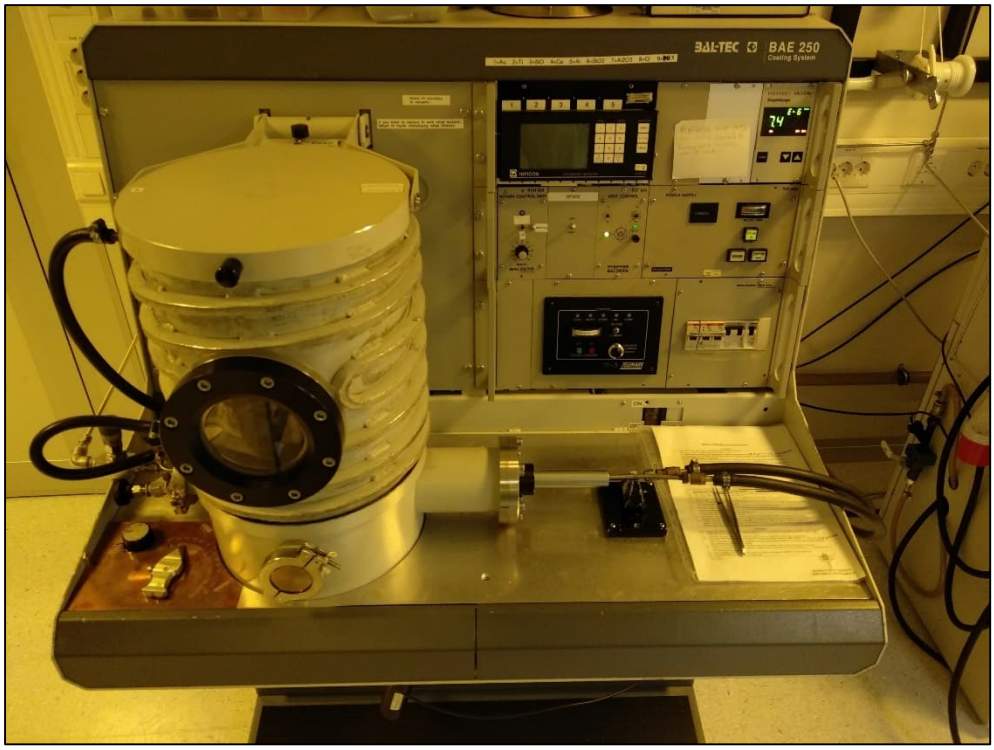

Figure 8 *The Balzers Baltec BAE 250 Vacuum e-beam evaporator at NSC used for Cu film deposition on Sapphire chips.*

After successfully evaporating Cu films on Sapphire chips, these are then transferred to the *GSL – 1100X* furnace (Figure 9) for graphene synthesis. Four Cu coated chips are first placed between two large clean sapphire pieces such that there is a gap between the top of the target (Cu coated) chips and the accompanying sapphire pieces (Figure 10). The arrangement is placed on a quartz ladle and inserted into the synthesis furnace through a load lock. It is to be noted that the chips are inserted into the furnace once it is at the right temperature and flushed with the annealing gases. The chips are annealed in the furnace at 1065 ºC for 10 - 15 minutes, to induce large Cu grain growth. After annealing, the graphene growth medium, Argon/Methane gas mixture (1% Methane, 4-8 sccm), is let into the furnace. The growth is also done at a temperature of 1065 ºC for 15-30 minutes depending on the Methane flow and adjusted based on the growth success of previous samples.

After the growth has been completed the sample holder is pulled towards the load lock and allowed to cool for about 5 minutes before being pulled into the load lock, where they are allowed to cool down further for the same time. Finally, the Graphene/Cu/Sapphire samples are moved out of the load lock and stored in a N_2 atmosphere holding cabinet.

The graphene growth is done by *lab technician, Olli Rissanen* and it is also to be noted that the temperatures listed for the graphene growth are read from the furnace sensors. The actual temperature inside the furnace tube is usually 10 – 15 ºC lower than what the sensor reads at such high temperatures.

Figure 9 *The GSL – 1100X furnace at NSC*

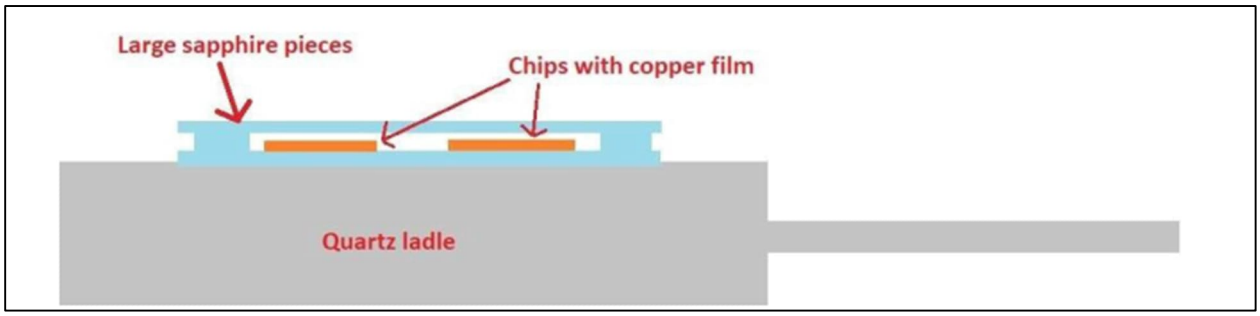

Figure 10 *Cu coated Sapphire chips between large Sapphire films placed on a quartz ladle before being placed inside the growth furnace.*

5.2 PMMA Assisted Transfer

After synthesizing graphene films on Cu coated Sapphire substrate, the Graphene-Cu-Sapphire stack was spin coated with PMMA-Anisole mixture at 4000 rpm using the *Laurell WS-650-23* spinner (Figure 11) which was then dried and baked on a hotplate at 150 ºC for 15 minutes. The edges of the PMMA layer are scraped off with a scalpel to make way for the

etchant to get under it in the next step. The Cu films were then etched by placing the chips in 0.5 M Ammonium Persulphate (APS) etchant overnight (Figure 11). After the etching, the sapphire substrate settles at the bottom and the detached PMMA-Graphene layer, which is left floating on the etchant surface, is scooped up and moved through 4 deionized water (DI) water baths. It is then suspended in a 12% HCl bath for about two minutes to get rid of any leftover debris or Cu residue under the films and put through a final DI water bath. The PMMA-Graphene layer is scooped up with the target substrate (SiO_2) from the final water bath. The PMMA-Graphene-SiO_2 stack is then baked at a temperature of 120 ºC to rid any moisture that might have been trapped under the graphene and substrate.

Finally, the PMMA layer is removed by dissolution in Acetone and Iso-propanol baths for 15 minutes each. The sample dried by blowing Nitrogen on the chips with an N_2 gun. The chips are then put through a two-step annealing in the GSL – 1100X furnace. First, in an Ar/H_2 (Ar, ~470 sccm and H_2 ~25 sccm) atmosphere at 300 ºC for 2 hours followed by annealing in an Oxygen (O_2, ~400 sccm) atmosphere at ~280 ºC for 1 hour.

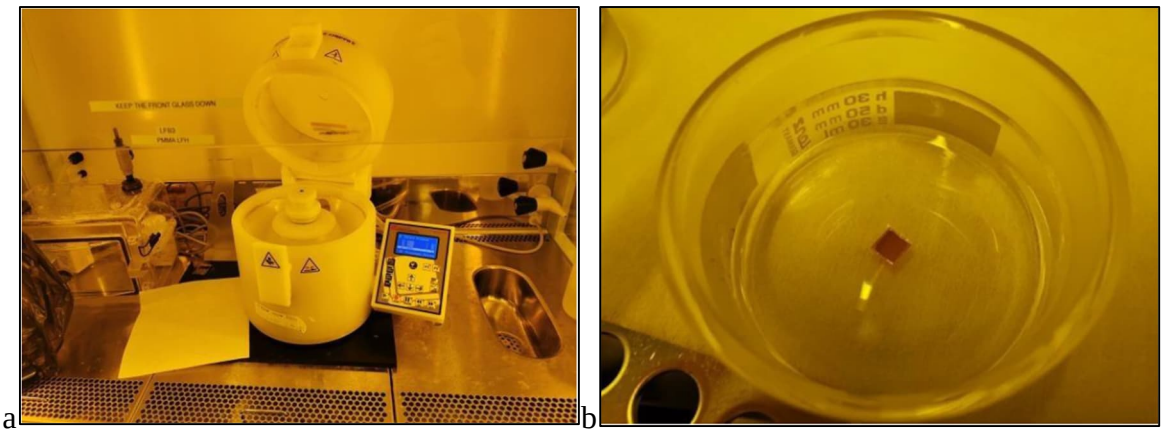

Figure 11 *a: Laurell WS-650-23 Spinner; b: A PMMA/Graphene/Cu/Sapphire stack floating in APS etchant.*

5.3 Paraffin Assisted Transfer

The paraffin assisted transfer procedure was adapted from the works of *Leong et. al. (2019)* and *Villa et. al. (2021).* The CVD grown Graphene-Cu-Sapphire stack is coated with Paraffin wax. The wax is kept in a molten state in a glass dish on top of a hotplate at about 80-90 ºC. The stack is put on the spinner stage while a heat-gun is held on top of it constantly blowing hot air towards the sample. A drop of the wax is then dropped on the sample while keeping the heat-gun running to keep it molten. The spinner is run at 1000-2000 rpm for different

samples for 90 seconds. *Table 1* lists the most significant paraffin assisted samples characterized and discussed here in this thesis alongside their spinning parameter. During the final 20 seconds of the spinning the heat gun is turned off to allow for the samples to gradually cool down during the spinning. After spinning, the samples are left untouched until the soft or molten paraffin film solidifies.

Table 1 *Paraffin deposition spin rate for different samples. The spinning time was 90 sec for all samples with an acceleration time of 10 sec.*

Sample	N0	N1	N2	N14	N15	N16	N17	Flipped	Settled
RPM	2.5k	1.5k	2k	1k	1.5k	1.5k	1k	1k	1k

The now Paraffin-Graphene-Cu-Sapphire stacks are placed in 0.5 M etchants for the Cu films to be etched away. The etching time was observed to be anywhere between 1-5 days. After the etching, the paraffin-graphene stack is scooped up and moved through four deionized water baths to get rid of any debris from the etching and then suspended in 12% HCl bath for about two minutes to get rid of any post etching Cu residue under the graphene. Later, the paraffin-graphene stack is moved through one last DI water bath from which it is scooped up with the target, SiO_2, substrate. For *Batch 1* of the samples (Section 6.3) the final DI water bath was heated to ~40 ºC in an attempt to expand the paraffin support layer and flatten it out further during the transfer.[5,7]

The paraffin-graphene-SiO_2 stacks are left to dry up overnight in the Nitrogen (N_2) holding cabinet. We did not bake the chips after transfer for the risk of softening the paraffin layer. We also observed some major bubble formation under the films during the baking hence, the drying was done at ambient temperatures. On the next day, the paraffin layer is dissolved by suspending the stack in 1M Hexane for 2 hours, followed by cleaning with Acetone and Iso-propanol baths and dried by blowing them with an N_2 gun. Finally, the samples were put through the same two-step annealing process the PMMA assisted samples were put through in Section 5.2 i.e., annealing at 300 ºC in an Ar/H_2 atmosphere for 2 hours followed by annealing in an O_2 atmosphere at 280 ºC for 1 hour.

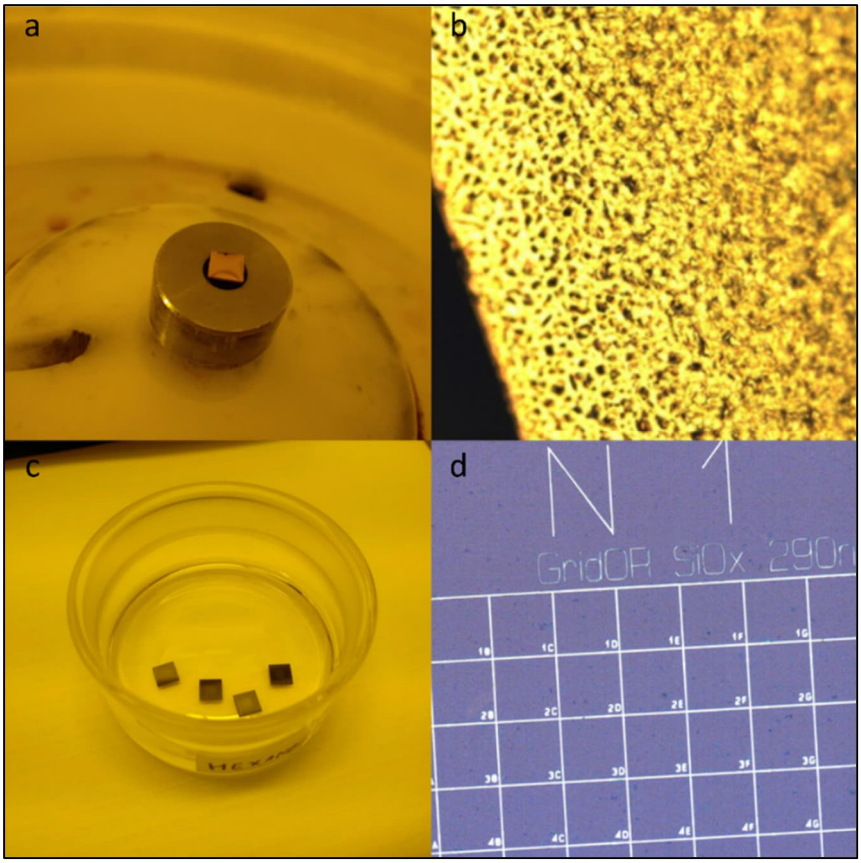

***Figure 12**, a: Molten paraffin solidifying after spinning; b: Paraffin film on top of a graphene/SiO_2 stack.; c: Paraffin film being dissolved in hexane; d: Final transferred graphene on SiO_2 (Not annealed).*

For the first batch of samples, the chips N0, N1 and N2 had paraffin coated at rpm's of 2500, 1500 and 2000 respectively, all for 90 seconds with an acceleration time of 10 seconds. *Batch 2* consisted of samples N14, N15, N16 and N17. Here, samples N14 and N17 were spin coated with paraffin at 1000 rpm for 90 seconds, while samples N15 and N16 were spin coated at 1500 rpm for 90 seconds. The acceleration time for batch two was also 10 seconds.

Batch 3 consisted of similar samples spun at 1000 rpm, with variations in how the stacks were suspended in APS during the Cu etching phase. One of the samples was settled at the bottom of the cup instead of the usual procedure where the stack is allowed to float on the etchant surface. Another sample was flipped upside down on etchant surface. These variations were made in order to see if the etching process was the cause of the cracks observed in the final graphene films due to the sapphire chips pulling on the floating graphene - paraffin stack before settling at the bottom of the etchant.

It is to be noted that the transfer attempts were made in chronological order for the three batches separately.

6. Results and Discussion

The first batch of samples consisted of chips N0, N1 and N2 that had graphene transferred on top of them by the assistance of a paraffin support layer. The PMMA transferred sample, discussed in *Section 5.2*, was used as a reference to compare the results of Raman Spectroscopy and Atomic Force Microscopy for both transfer procedures. Numerous transfer attempts were made for transferring graphene with paraffin as a support layer. In the upcoming sections, we discuss the most significant samples observed.

For Raman Spectroscopy, we used the *Thermo Fisher DXR Raman Microscope* and the samples were subjected to an excitation wavelength of 532 nm. The beam power was set at 5 mW and a pinhole size of 50 µm was used. The Raman spectra comparison was made for samples in both pre-annealed and post-annealed states to get an idea about how the annealing process affected the graphene quality. For AFM imaging we used the *Bruker Dimension icon ScanAsyst* AFM setup (Figure 7). For the sake of consistency, we tried to image approximately the same chosen area on each sample for both AFM and Raman. The AFM images were taken after annealing the samples for the best possible results for both PMMA and Paraffin assisted Graphene.

6.1 Batch 1 (N0, N1 & N2)

The optical microscope images for the most notable samples in this batch, N0, N1 and N2 alongside the reference PMMA assisted sample, are shown below (Figure 13). The paraffin support layer failed to preserve the film integrity on a larger scale. The PMMA assisted reference sample appears much more intact and cleaner looking under the optical microscope. The Paraffin assisted graphene films have a lot of debris accumulated underneath them. We also see remnants of paraffin on them as well as some unidentified foreign particles. However, a closer look under the AFM and Raman Microscope reveals that paraffin still appears to hold some advantage over PMMA as discussed below. We chose, what seemed to be the cleanest areas on the films by visual inspection for the characterizations.

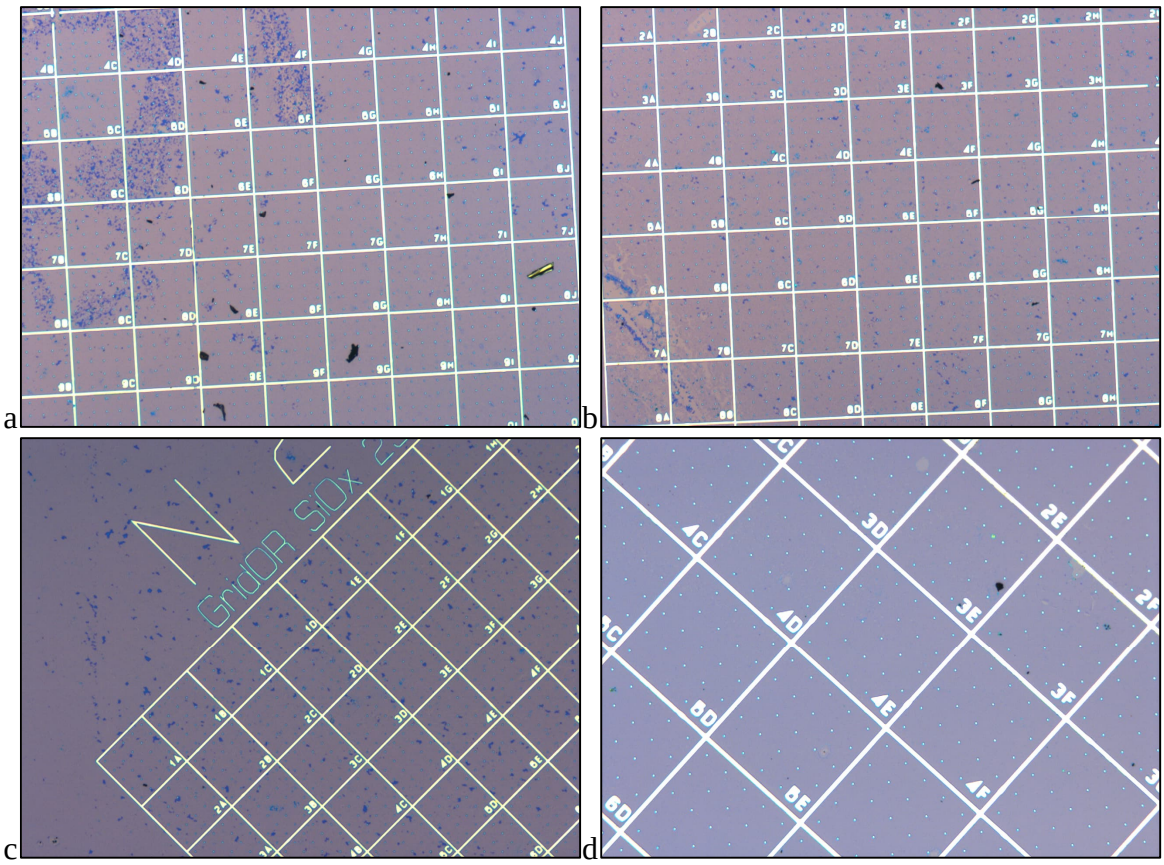

Figure 13 *Batch 1 Optical Microscope Images after transfer, a: Sample N0; b: Sample N1; c: Sample N2; d: Reference PMMA assisted sample.*

For sample **N0**, the Raman spectra (Figure 14a and 14b) shows the least D-band intensity for the non-annealed paraffin transferred sample (Red) in comparison to the annealed PMMA (Blue) and non-annealed PMMA (Black) assisted transfers. The non-annealed PMMA assisted sample shows a higher D-band intensity, showcasing higher residue and contaminants in addition to structural defects in graphene. This is not ideal for high performance graphene use. After annealing, for both PMMA and paraffin transferred graphene samples, the D-bands show an increase in intensity, which we speculate to be due to the contaminants in the annealing furnace and foreign particles on the film surface that resulted in unnecessary doping of the sample. The D-bands also shift more towards the ideal 1350cm^{-1} Raman Shift, which indicates a higher degree of graphitization and order in the films.

The AFM images show a high number of wrinkles in the PMMA transferred graphene (Figure 15). The paraffin transferred graphene layers (Figure 14c and 14d) remained intact with lower wrinkle density for the scanned area. It also appeared a lot cleaner with some paraffin residue and foreign particle deposits observed.

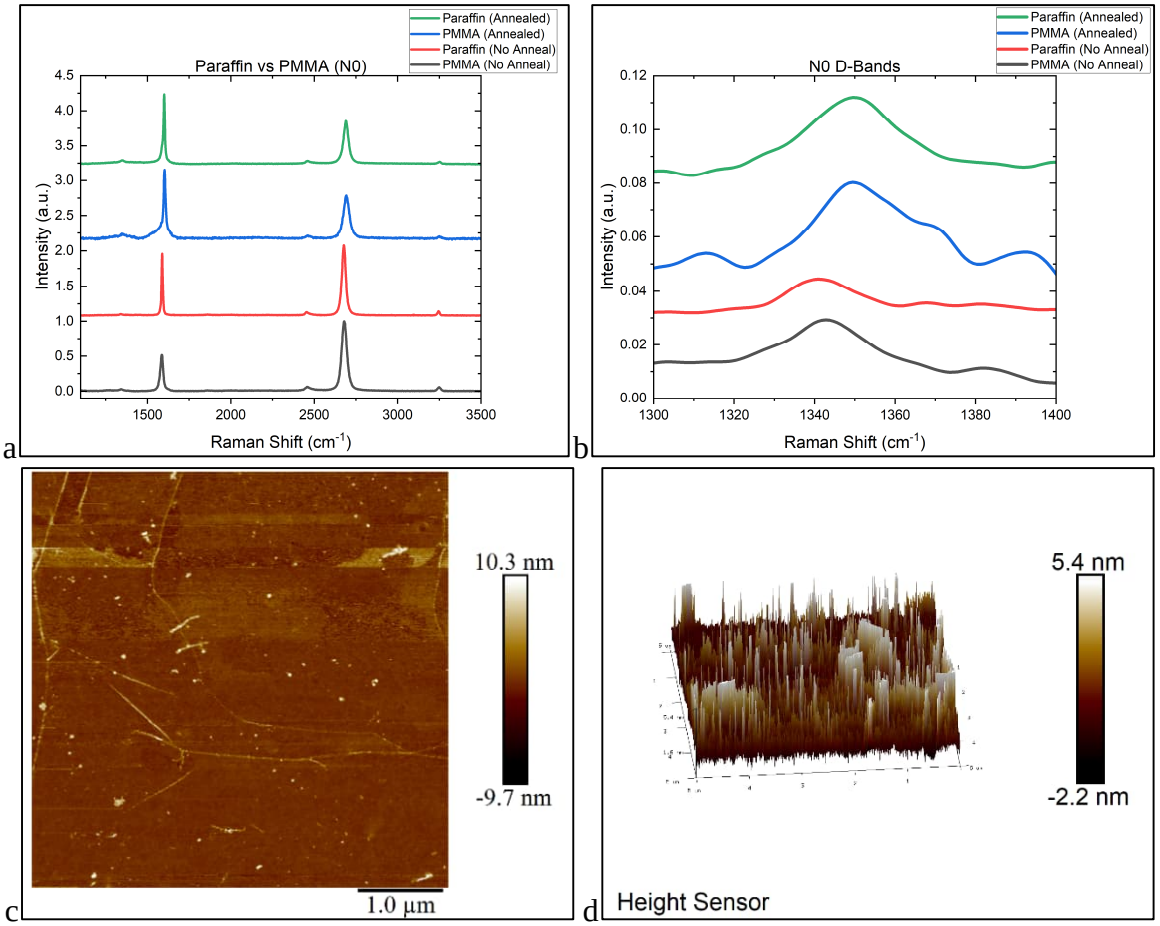

***Figure 14**, Sample N0 Film Characterization: a: Raman Spectra for reference PMMA transferred film pre-anneal (black), paraffin assisted N0 pre-anneal(red), reference PMMA assisted post-anneal (blue) and paraffin assisted N0 post anneal (green); b: D-Band comparison for PMMA and Paraffin assisted graphene; c: AFM image for N0; d: 3-D AFM data for N0.*

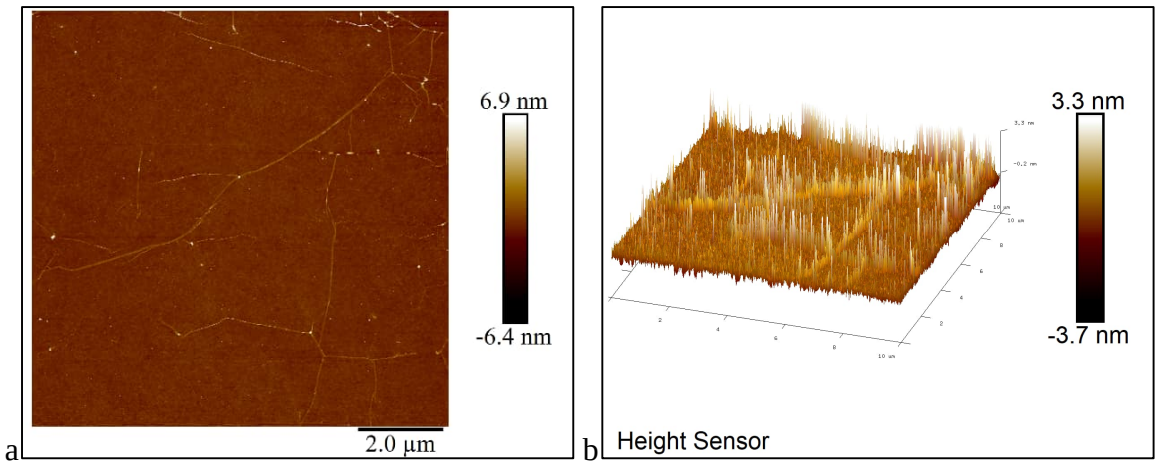

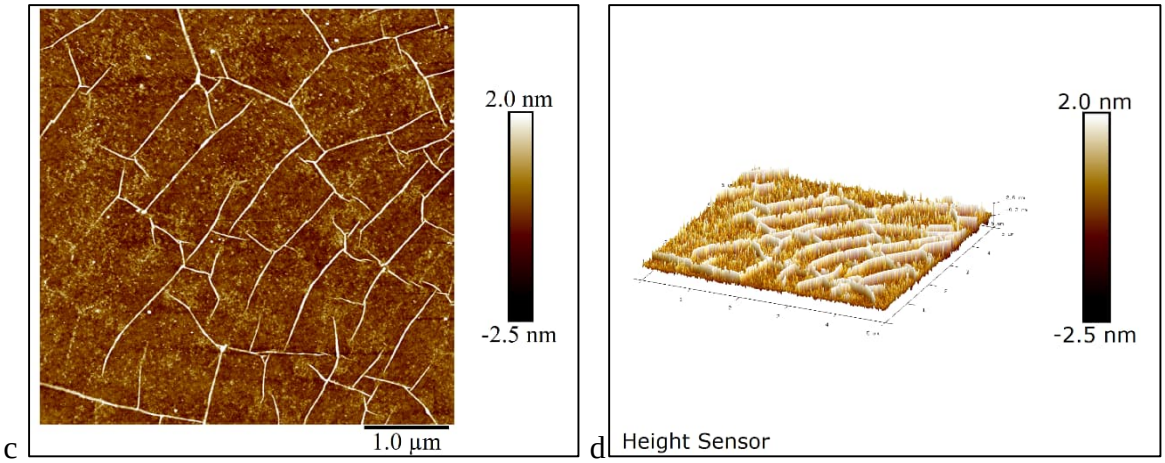

Figure 15 *Reference PMMA assisted transferred graphene sample imaged under AFM at two different spots. a: Spot 1, 2-D AFM image; b: Spot 1, 3-D AFM data; c: Spot 2, 2-D AFM image; d: Spot 2, 3-D AFM data.*

Sample **N1** (Figure 16) veered away from the observations made for N0. It appeared that the non-annealed PMMA transferred films were relatively cleaner as compared to its paraffin counterpart. We can still notice the same amount of doping for both the films post annealing. The AFM image showed a considerable number of cracks, folds and wrinkles in the paraffin assisted sample.

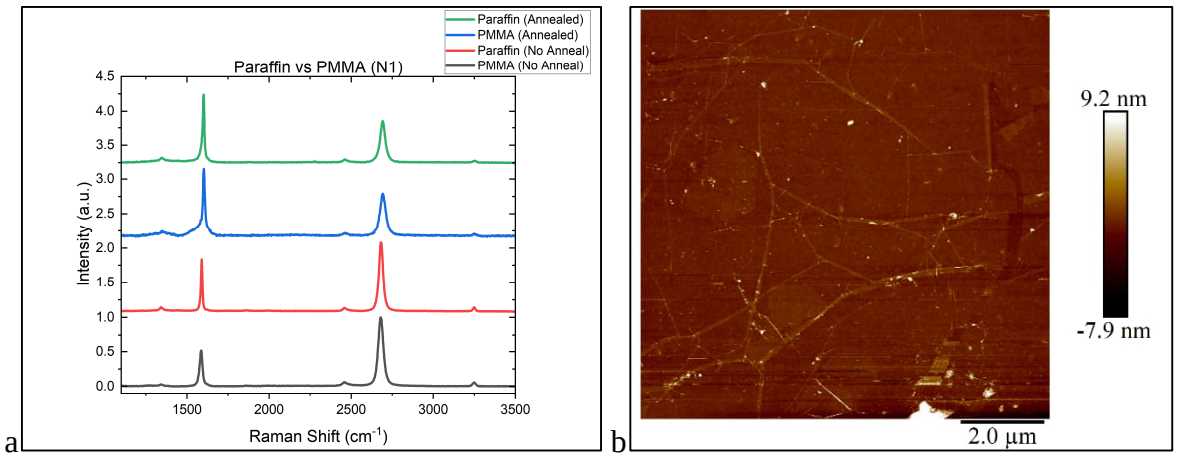

Figure 16 *Sample N1 Characterization, a: Raman Spectra for N1; b: AFM 2-D Image for N1*

N2 showed similar behavior to N1 above. There was severe damage to the graphene layer during transfer with observable cracks, folds, and pieces of graphene missing (Figure 17c and 17d). The D-band comparison (Figure 17b) also shows that the non-annealed PMMA assisted graphene layer (black) had lower peak intensity in comparison to the paraffin (Red). On the

other hand, it seems slightly wider, which is common when there is a larger variety of defects with different vibrational modes. The higher contamination of the paraffin assisted graphene can also be due to the debris under the layer accumulated due to the longer etching times.

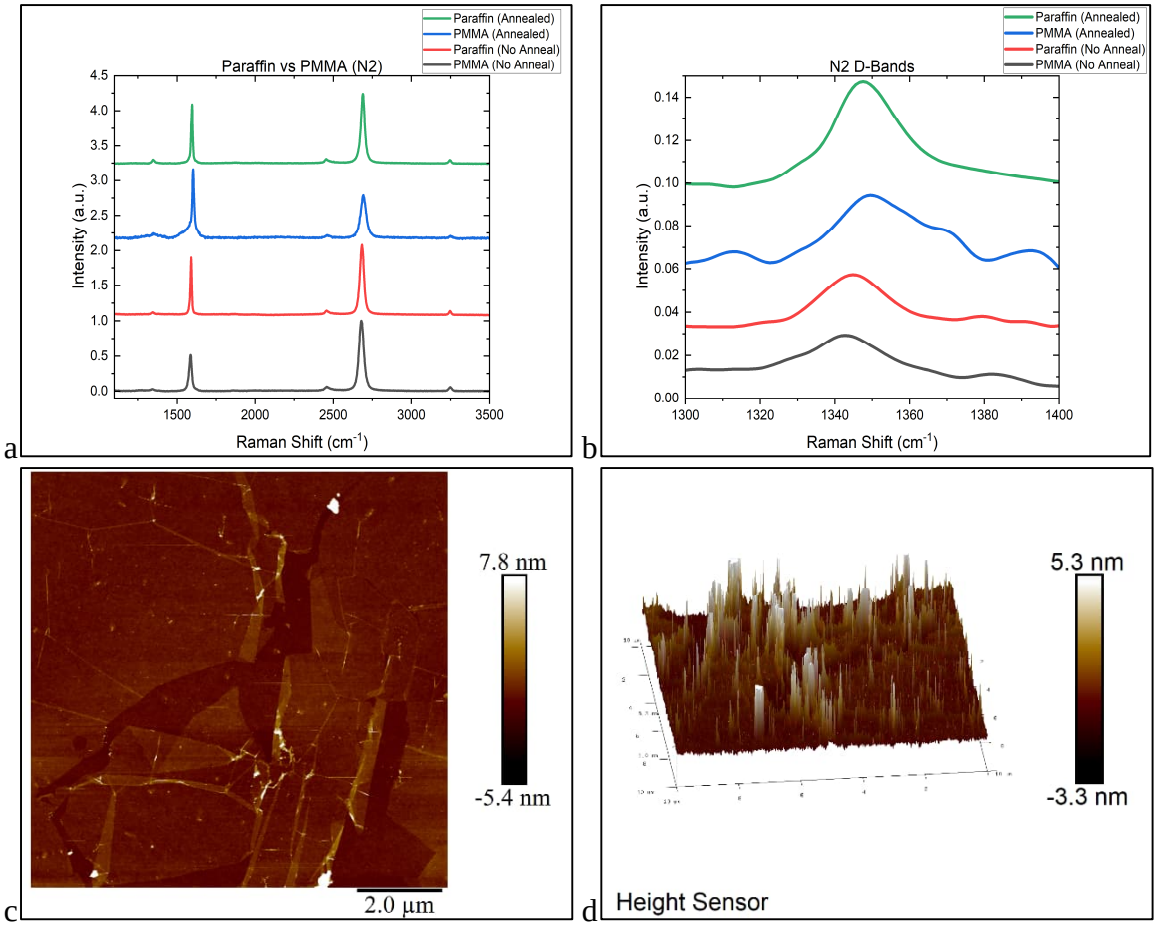

Figure 17 *Sample N2 Film Characterization: a: Raman Spectra for reference PMMA transferred film pre-anneal (black), paraffin assisted N0 pre-anneal(red), reference PMMA assisted post-anneal (blue) and paraffin assisted N0 post anneal (green); b: D-Band comparison for PMMA and Paraffin assisted graphene; c: AFM image for N2; d: 3-D AFM data for N2.*

After Batch 1, it was concluded that spinning paraffin at rpm's higher than 1.5k resulted in too thin of a support film which was the least effective in preserving the graphene layer integrity during transfers. Hence, for the following batches, spin rates of 1500 rpm or lower were used. Moreover, the heating of the final DI water bath before scooping up the paraffin-graphene stack was eliminated to account for potential cracking of graphene due to thermal over-expansion of paraffin.

6.2 Batch 2 (N14, N15, N16 & N17)

The optical microscope images for this batch are shown below (Figure 18). We notice similar fragmentation as observed in Batch 1 but there were some bigger more intact areas that could be imaged.

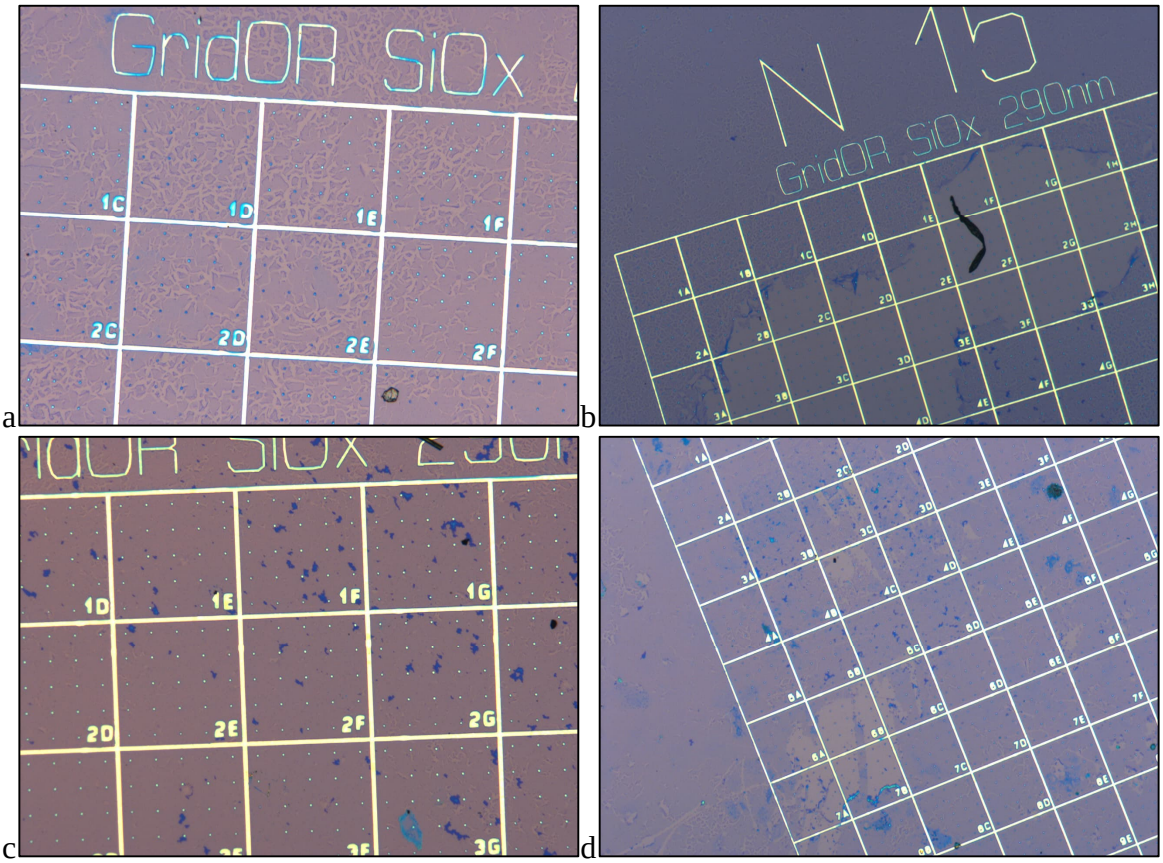

a b c d

Figure 18 *Batch 2 Optical Microscope Images after transfer, a: Sample N14; b: Sample N15; c: Sample N16; d: Sample N17*

The Raman spectra for chip **N14** (Figure 19a) shows non-annealed paraffin assisted graphene layer (Red) to exhibit the lowest contamination, with an almost flat D-band (at ~ 1350 cm^{-1}) (Figure 19b) indicating the least amount of residue and contaminants on the layer. The PMMA assisted layer (Black) shows a higher D-band intensity indicating a higher amount of leftover residue (from PMMA film) or other contaminants. Since the paraffin and PMMA transfers were done under similar conditions the differentiating factor can be assumed to be just the respective support film residues. The lower intensity of the 2D band (at ~ 2700 cm^{-1}) can be attributed to the flattening of the graphene layer after annealing, leading to enhanced

interaction with the substrate and stronger doping. For post-annealed paraffin assisted graphene, the D-band shifts towards > 1340 cm^{-1} indicating an increase in disorder.

The AFM 2-D and 3-D images (Figure 19c and 19d) for N14 also show a much cleaner and flatter graphene layer with most of the imaged area intact and very little paraffin residue. We only see two noticeable cracks in the final graphene layer near the bottom edge.

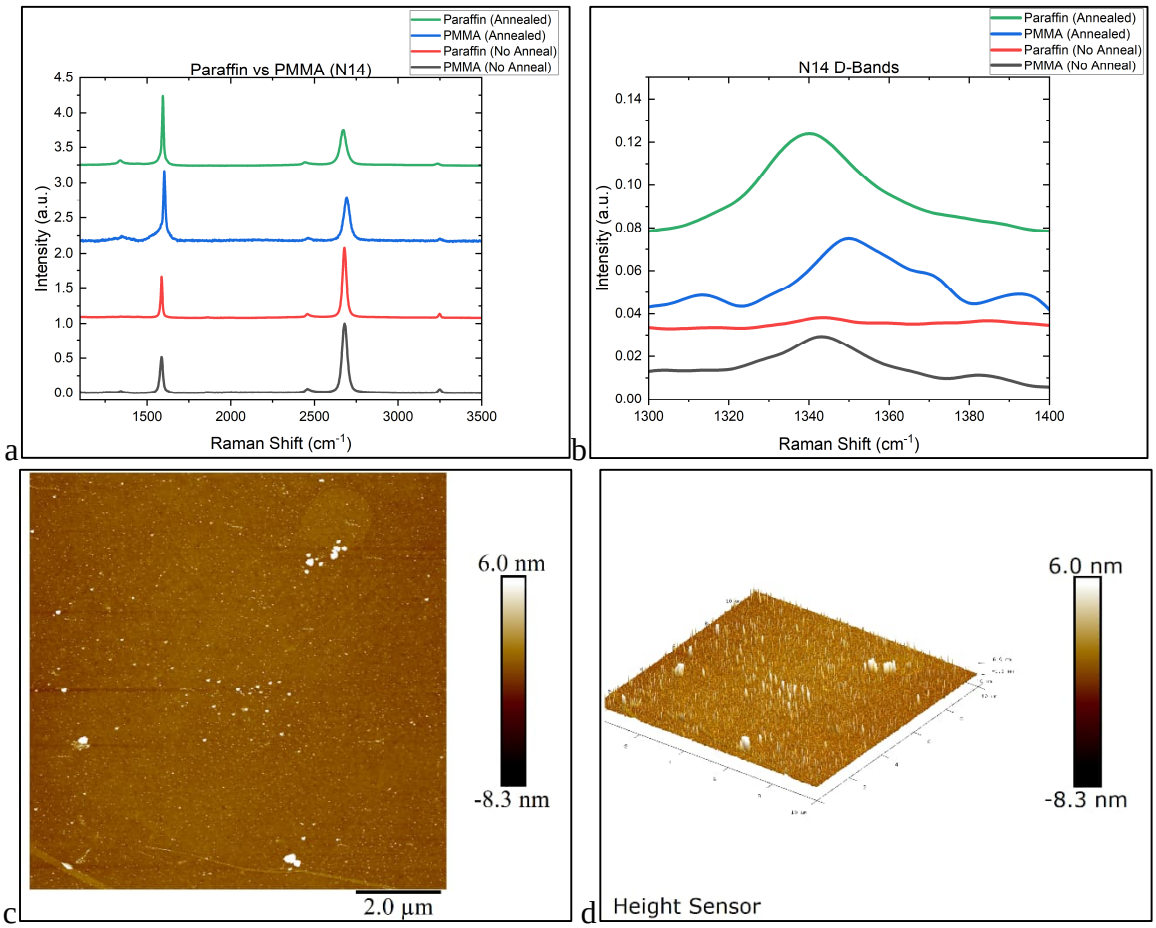

Figure 19 *Sample N14 Film Characterization, a: Raman Spectra for reference PMMA transferred film pre-anneal (black), paraffin assisted N0 pre-anneal(red), reference PMMA assisted post-anneal (blue) and paraffin assisted N14 post anneal (green); b: D-Band comparison for PMMA and Paraffin assisted graphene; c: AFM image for N14; d: 3-D AFM data for N14.*

N15 AFM images (Figure 20a and 20b) showed some severe damage to the graphene on one side while the overall integrity of the layer was still conserved in the remaining imaged area. The intact area still appears much cleaner than what was observed for the PMMA assisted graphene. The Raman spectra shows a higher D-band intensity for paraffin assisted samples here for both pre- and post-annealing conditions (figure 20c and 20d). The D-band position > 1340 cm^{-1} here again shows a high degree of disorder.

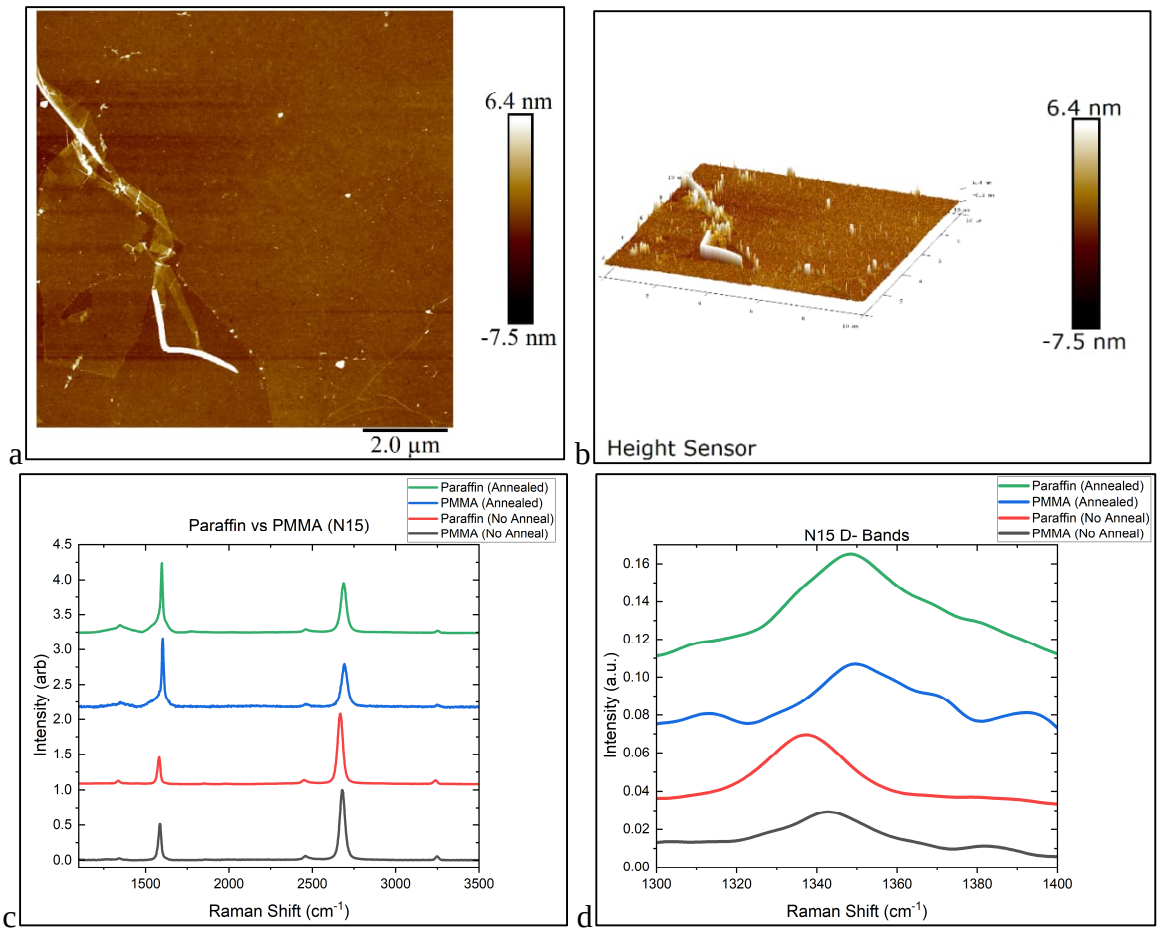

Figure 20 *Sample N15 Film Characterization, a: AFM image for N15; b: 3-D AFM data for N15; c: Raman Spectra for reference PMMA transferred film pre-anneal (black), paraffin assisted N0 pre-anneal(red), reference PMMA assisted post-anneal (blue) and paraffin assisted N15 post anneal (green); d: D-Band comparison for PMMA and Paraffin assisted graphene.*

N16 (Figure 21a and 21b) showed similar behavior as N15, with little difference between the D-band intensities and shape. There was an addition of higher paraffin residue on the layer and contamination leading to a much higher doping for the paraffin assisted sample post-annealing. The D-band positions (< 1340 cm^{-1}) indicate a high order of defect and disorder density in the graphene layer even after annealing here.

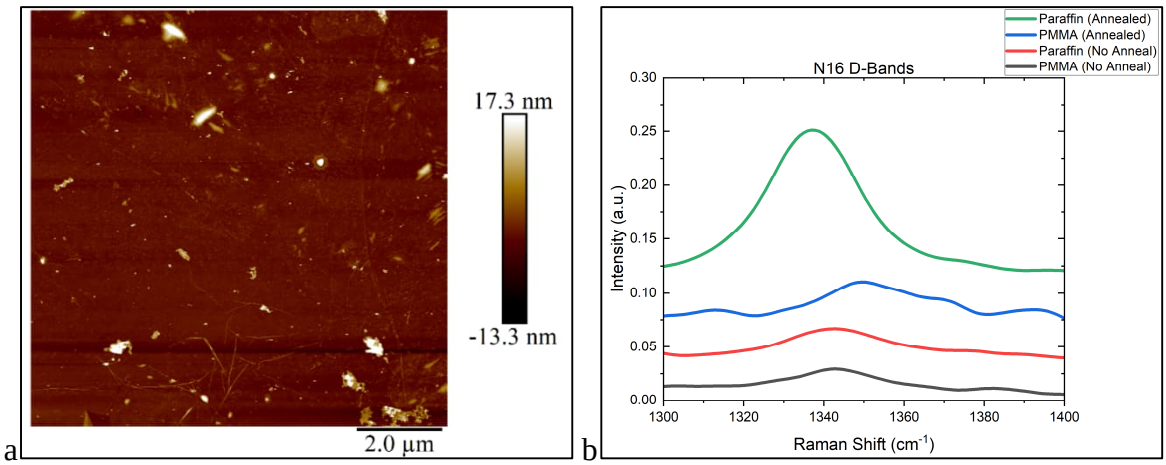

Figure 21 *Sample N16 film characterization, a: AFM 2-D image; b: D-band comparison for PMMA and Paraffin assisted graphene both pre- and post-annealing.*

N17 seemed to preserve the film integrity but the AFM 2-D image and 3-D data (Figure 22a and 22b) show the highest paraffin residue observed out of any of the samples. This seems to have been a one-off case since no such behavior was observed in any other transfer attempts. The Raman spectra exhibited similar post annealing doping behavior as N16 while the pre-annealed graphene layers for both PMMA and paraffin showed similar intensity and shapes indicating similar purity factors (Figure 22c and 22d).

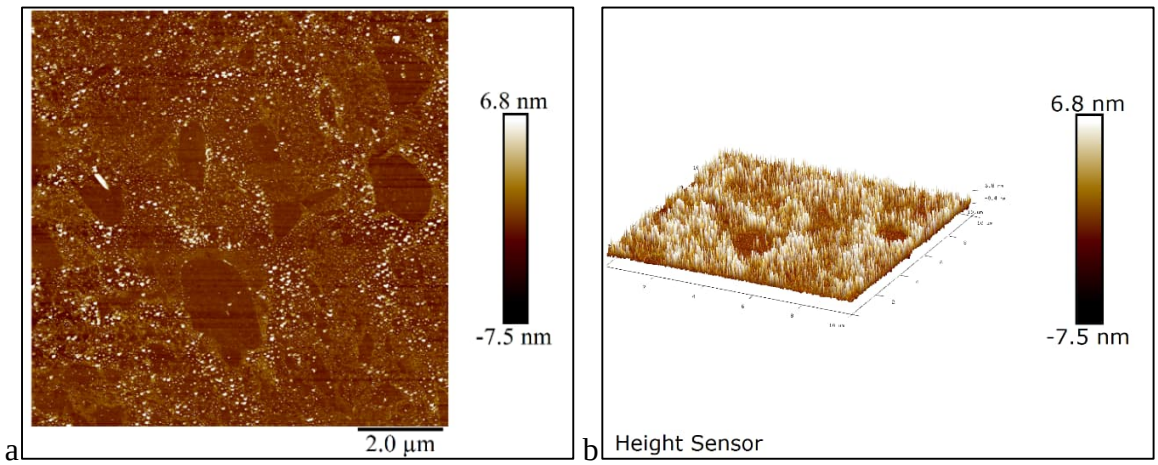

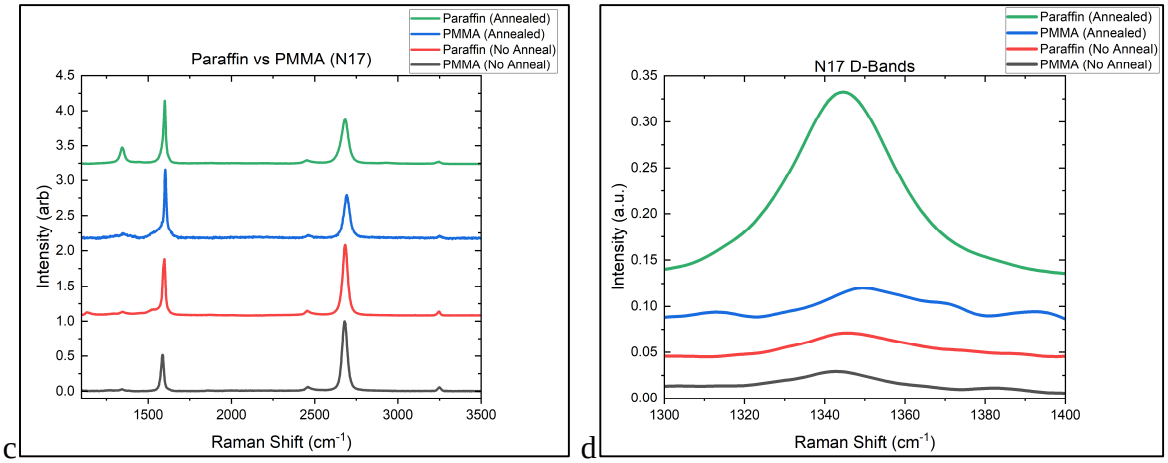

Figure 22 *Sample N17 Film Characterization, a: AFM image for N17; b: 3-D AFM data for N17; c: Raman Spectra for reference PMMA transferred film pre-anneal (black), paraffin assisted N0 pre-anneal(red), reference PMMA assisted post-anneal (blue) and paraffin assisted N17 post anneal (green); d: D-Band comparison for PMMA and Paraffin assisted graphene.*

6.3 Batch 3 (Flipped & Settled)

The first two iterations of the transfer experiments (Batch 1 & 2) showed a high occurrence of film damage during transfer. The different paraffin thicknesses on the samples showed varying results with the graphene layers remaining intact at spin rates of 1000 rpm and 1500 rpm (see Table 1) but there was still some damage observed. We speculated that the damage to the graphene layer might have occurred during the Cu film etching in APS due to the sapphire chip pulling down on the paraffin – graphene stack before settling at the bottom of the etchant.

So, for Batch 3, we tried letting one sample sit at the bottom of the etchant and another flipped over but still left to float on the etchant surface. In our further discussion, the samples will be referred to as *"Settled"* and *"Flipped"* respectively. Both the samples were coated with paraffin at 1000 rpm for 90 seconds.

The optical microscope images for the two are shown below (Figure 23). These showed the most "large"-scale graphene layer integrity we had observed so far with Paraffin support films, though still fragmented and not as clean looking as its PMMA counterparts. (Figure 13d).

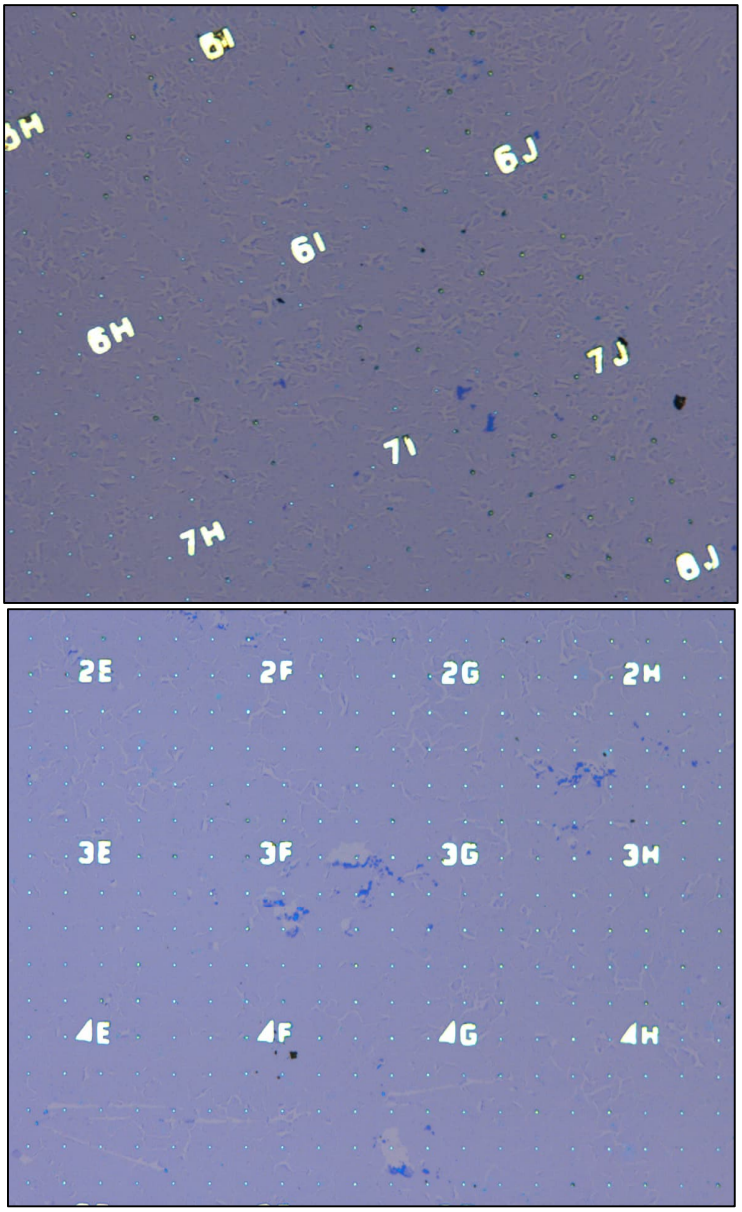

Figure 23 *Batch 3 Optical Microscope Images after transfer, Top: 'Flipped' sample which was allowed to float on the APS etchant surface with the sapphire chip facing up.; Bottom: 'Settled' sample which was allowed to settle at the bottom of the APS cup during etching.*

The AFM images for the *Flipped* sample (Figure 24a and 24b) showed the graphene layer to be intact for the most part with less cracks and wrinkles compared to its PMMA assisted counterpart. There are still residues observed for the respective support layers, but the paraffin supported layer appears much cleaner.

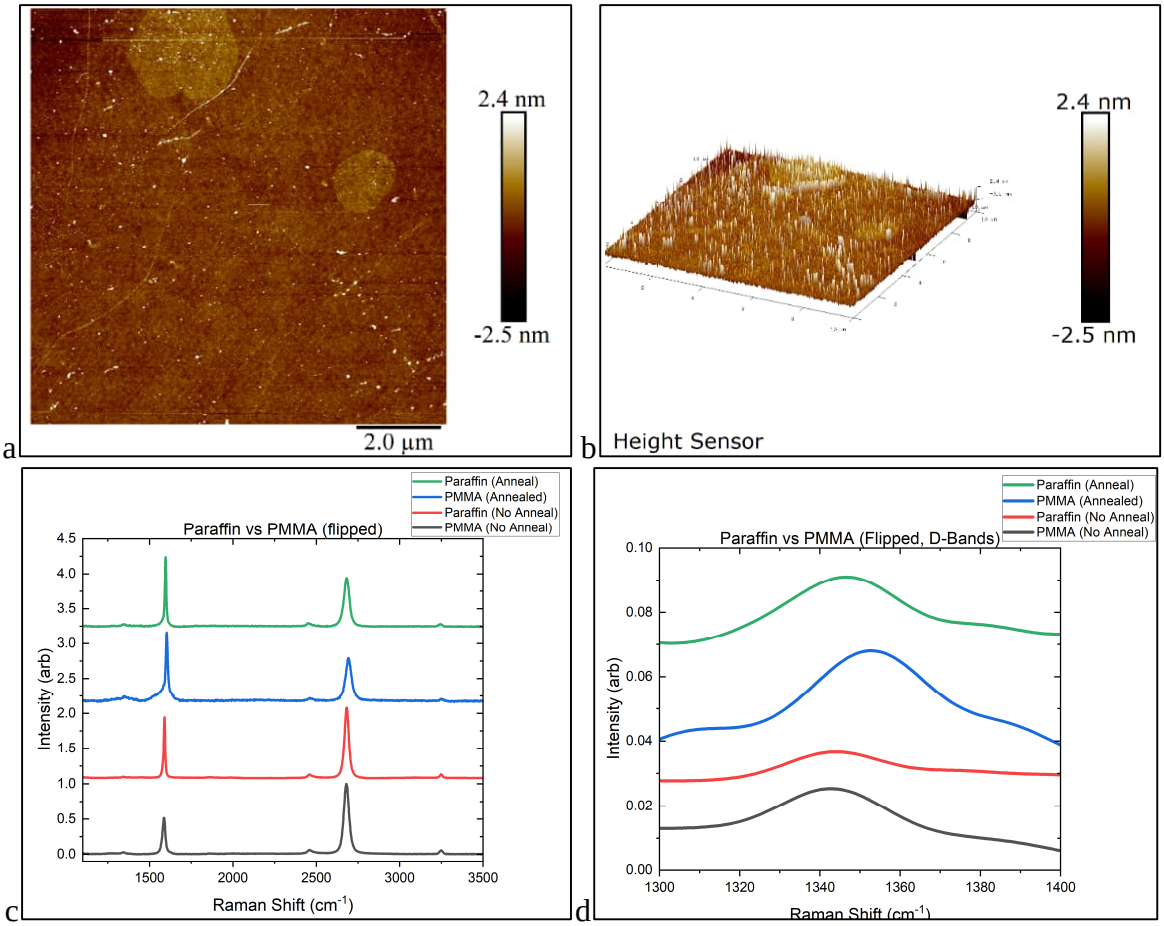

Figure 24 *Flipped sample Film Characterization, a: AFM image for 'flipped'; b: 3-D AFM data for 'flipped'; c: Raman Spectra for reference PMMA transferred film pre-anneal (black), paraffin assisted N0 pre-anneal(red), reference PMMA assisted post-anneal (blue) and paraffin assisted 'flipped' post anneal (green); d: D-Band comparison for PMMA and Paraffin assisted graphene.*

The Raman spectra for the Flipped (Figure 24c and 24d) sample again shows the paraffin assisted graphene to be much less contaminated with the non-annealed paraffin assisted sample showing the lowest D- band intensity peak while the same for PMMA assisted samples were higher and the band was much wider as well. After annealing similar doping effects were observed as all the samples above but the overall D-band intensity for paraffin assisted sample was still lower.

The *Settled* sample turned out to be our most successful paraffin assisted transfer out of all the attempts made so far. The AFM image shows only two observable cracks for a scan size of 10 µm and no visible wrinkles in the layer (Figure 25a and 25b). The paraffin film residue was also the lowest we observed out of all the transfer attempts made and comparatively far lower than the polymer residue observed in PMMA assisted graphene.

The Raman Spectra for the settled sample also shows the pre-annealed D-band as almost flat, hinting at little to no contamination of the graphene layer in the excited areas of the film (Figure 25c and 25d).

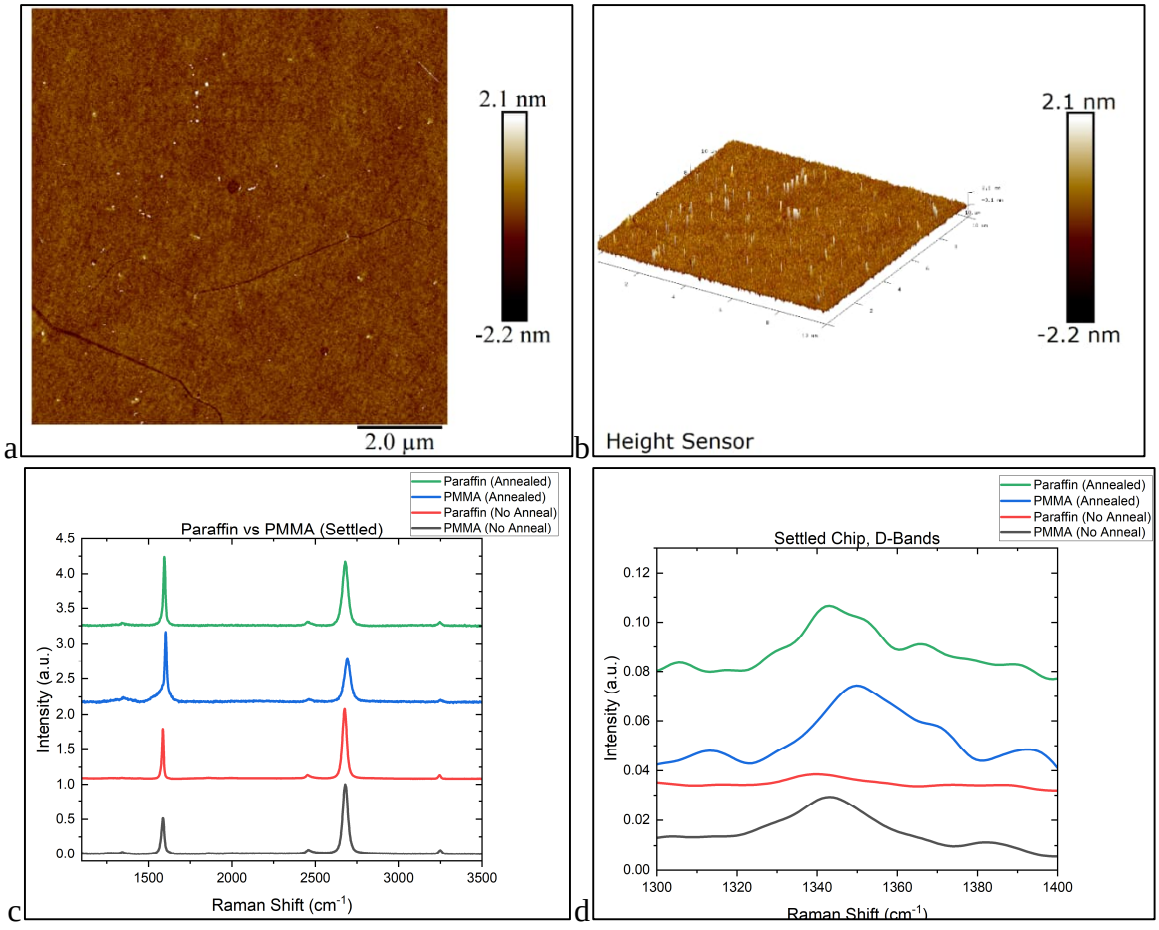

Figure 25 *'Settled' Sample Film Characterization, a: AFM image for 'settled'; b: 3-D AFM data for 'settled'; c: Raman Spectra for reference PMMA transferred film pre-anneal (black), paraffin assisted N0 pre-anneal(red), reference PMMA assisted post-anneal (blue) and paraffin assisted 'settled' post anneal (green); d: D-Band comparison for PMMA and Paraffin assisted graphene.*

7. Conclusions

We were able to prove the effectiveness of Paraffin as a support layer for transferring CVD synthesized graphene to obtain cleaner films. Our results show that the majority of the transferred graphene films had considerably less residue post removal than what is observed in PMMA assisted transfers. While the imaged paraffin samples were wrinkle and crack free to some degree for smaller scan sizes, with deformations being much less frequent than PMMA assisted transfers, large area paraffin assisted graphene transfer was not achieved to the extent of what is currently attainable through PMMA. This is evident from the optical

images shown in the results and discussion section. The cracks and fragmentation observed in the paraffin assisted graphene can be due to several factors that need to be monitored more closely. For example, uneven heating from the heat-gun during spinning, forces induced during the etching phase or the transfer phase.

But perhaps the results are satisfactory enough to start looking forward to using paraffin as a replacement for PMMA on a smaller, laboratorial scale. We tried various spin rates and paraffin film thicknesses to see how effective the support layer was in holding the graphene intact during transfers. It is recommended for future trials to spin at rates between 1000-1500 rpm when depositing paraffin on graphene. In addition, we recommend that the samples be allowed to settle at the bottom of the etchant during the Cu film etching phase since it resulted in the best transfer result we observed.

For future research, further optimization of the etching process is needed since it took almost up to a week for Cu etching during our experiments. We would also recommend experimenting with a mix of Paraffin/Hexane solution for depositing the support layer rather than pure paraffin as done in our work above. Once achieved, Paraffin assisted large area graphene transfer can be a reliable and effective alternative for transferring high quality graphene, with the obtained films being much cleaner, flatter, and devoid of defects or damage. Carrier mobility measurements can also be conducted for both PMMA and Paraffin assisted graphene to compare performance differences. Furthermore, Paraffin assisted transfer can possibly be utilized for advancing graphene related research, such as multilayer graphene stacking and alignment.

8. References

1. Novoselov, K. S. *et al.* Electric field in atomically thin carbon films. *Science (1979)* **306**, 666–669 (2004).

2. Geim, A. K. & Novoselov, K. S. *The rise of graphene*. www.nature.com/naturematerials.

3. Inagaki, M., Kang, F., Toyoda, M. & Konno, H. Graphene: Synthesis and Preparation. *Advanced Materials Science and Engineering of Carbon* 41–65 (2014) doi:10.1016/B978-0-12-407789-8.00003-X.

4. Miller, D. L. *et al.* Giant secondary grain growth in Cu films on sapphire. *AIP Adv* **3**, 82105 (2013).

5. Villa, N., Zapata, J. D. & Ramirez, D. Paraffin wax assisted chemical vapor deposited graphene transfer method. *Thin Solid Films* **721**, 138556 (2021).

6. Chen, M., Haddon, R. C., Yan, R. & Bekyarova, E. Advances in transferring chemical vapour deposition graphene: A review. *Mater Horiz* **4**, 1054–1063 (2017).

7. Leong, W. S. *et al.* Paraffin-enabled graphene transfer. *Nature Communications 2019 10:1* **10**, 1–8 (2019).

8. Lu, W., Soukiassian, P. & Boeckl, J. Graphene: Fundamentals and functionalities. *MRS Bull* **37**, 1119–1124 (2012).

9. Chen, J. *et al.* Nanomechanical properties of graphene on poly(ethylene terephthalate) substrate. *Carbon N Y* **55**, 144–150 (2013).

10. Joh, H. I., Lee, S., Kim, T. W., Hwang, S. Y. & Hahn, J. R. Synthesis and properties of an atomically thin carbon nanosheet similar to graphene and its promising use as an organic thin film transistor. *Carbon N Y* **55**, 299–304 (2013).

11. Min, K. & Aluru, N. R. Mechanical properties of graphene under shear deformation. *Appl Phys Lett* **98**, 43 (2011).

12. Rahat Rahman, M., Rashid, Md. M., Islam, Md. M. & Akanda, Md. M. Electrical and Chemical Properties of Graphene over Composite Materials: A Technical Review. *Material Science Research India* **16**, 142–163 (2019).

13. Carlsson, J. M., Hanke, F., Linic, S. & Scheffler, M. Two-Step Mechanism for Low-Temperature Oxidation of Vacancies in Graphene. *Phys Rev Lett* **102**, 166104 (2009).

14. Smith, A. T., LaChance, A. M., Zeng, S., Liu, B. & Sun, L. Synthesis, properties, and applications of graphene oxide/reduced graphene oxide and their nanocomposites. *Nano Materials Science* **1**, 31–47 (2019).

15. Pinto, A. M., Gonçalves, I. C. & Magalhães, F. D. Graphene-based materials biocompatibility: A review. *Colloids Surf B Biointerfaces* **111**, 188–202 (2013).

16. Mohan, V. B., Brown, R., Jayaraman, K. & Bhattacharyya, D. Characterisation of reduced graphene oxide: Effects of reduction variables on electrical conductivity. *Materials Science and Engineering: B* **193**, 49–60 (2015).

17. Hummers, W. S. & Offeman, R. E. Preparation of Graphitic Oxide. *J Am Chem Soc* **80**, 1339 (1958).

18. McAllister, M. J. *et al.* Single sheet functionalized graphene by oxidation and thermal expansion of graphite. *Chemistry of Materials* **19**, 4396–4404 (2007).

19. Yu, Q. *et al.* Graphene segregated on Ni surfaces and transferred to insulators. *Appl Phys Lett* **93**, (2008).

20. Li, X. *et al.* Large-area synthesis of high-quality and uniform graphene films on copper foils. *Science (1979)* **324**, 1312–1314 (2009).

21. Chen, X., Zhang, L. & Chen, S. Large area CVD growth of graphene. *Synth Met* **210**, 95–108 (2015).

22. Garcia, J. M. *et al.* Graphene growth on h-BN by molecular beam epitaxy. *Solid State Commun* **152**, 975–978 (2012).

23. Park, J. *et al.* Epitaxial Graphene Growth by Carbon Molecular Beam Epitaxy (CMBE). *Advanced Materials* **22**, 4140–4145 (2010).

24. Qin, H., Sun, Y., Liu, J. Z. & Liu, Y. Mechanical properties of wrinkled graphene generated by topological defects. *Carbon N Y* **108**, 204–214 (2016).

25. Chen, M. *et al.* Sublimation-assisted graphene transfer technique based on small polyaromatic hydrocarbons. *Nanotechnology* **28**, 255701 (2017).

26. Barin, G. B. *et al.* Optimized graphene transfer: Influence of polymethylmethacrylate (PMMA) layer concentration and baking time on graphene final performance. *Carbon N Y* **84**, 82–90 (2015).

27. Li, X. *et al.* Transfer of large-area graphene films for high-performance transparent conductive electrodes. *Nano Lett* **9**, 4359–4363 (2009).

28. P Morin, J. L. *et al.* Dry transfer of chemical-vapor-deposition-grown graphene onto liquid-sensitive surfaces for tunnel junction applications. *Nanotechnology* **26**, 035302 (2014).

29. Chen, M. *et al.* Large-scale cellulose-assisted transfer of graphene toward industrial applications. *Carbon N Y* **110**, 286–291 (2016).

30. Samavedi, S., Poindexter, L. K., Van Dyke, M. & Goldstein, A. S. Synthetic Biomaterials for Regenerative Medicine Applications. *Regenerative Medicine Applications in Organ Transplantation* 81–99 (2014) doi:10.1016/B978-0-12-398523-1.00007-0.

31. Babo, S. *et al.* Characterization and Long-Term Stability of Historical PMMA: Impact of Additives and Acrylic Sheet Industrial Production Processes. *Polymers 2020, Vol. 12, Page 2198* **12**, 2198 (2020).

32. Yu, Y. & Wang, J. Preparation of graphene/PMMA composites with assistance of ultrasonic wave under supercritical CO2 conditions. *Ultrason Sonochem* **73**, 105487 (2021).

33. Kim, S. *et al.* Robust graphene wet transfer process through low molecular weight polymethylmethacrylate. *Carbon N Y* **98**, 352–357 (2016).

34. Speight, J. G. Hydrocarbons from Petroleum. *Handbook of Industrial Hydrocarbon Processes* 85–126 (2011) doi:10.1016/B978-0-7506-8632-7.10003-9.

35. Kumar, D. *et al.* Raman Spectroscopy in Nanotechnology Applications. *Int J Acad Res* **4**, 2348–7666 (2017).

36. Cong, X., Liu, X. L., Lin, M. L. & Tan, P. H. Application of Raman spectroscopy to probe fundamental properties of two-dimensional materials. *npj 2D Materials and Applications 2020 4:1* **4**, 1–12 (2020).

37. Ferrari, A. C. & Basko, D. M. Raman spectroscopy as a versatile tool for studying the properties of graphene. *Nature Nanotechnology 2013 8:4* **8**, 235–246 (2013).

38. Malard, L. M., Pimenta, M. A., Dresselhaus, G. & Dresselhaus, M. S. Raman spectroscopy in graphene. *Phys Rep* **473**, 51–87 (2009).

39. Wall, M. Raman spectroscopy optimizes graphene characterization. *Advanced Materials and Processes* **170**, 35–38 (2012).

40. Eaton, P. Atomic Force Microscopy–AFM. *Kirk-Othmer Encyclopedia of Chemical Technology* 1–19 (2011) doi:10.1002/0471238961.0120151319011809.A01.PUB2.

41. Sinha Ray, S. Structure and Morphology Characterization Techniques. *Clay-Containing Polymer Nanocomposites* 39–66 (2013) doi:10.1016/B978-0-444-59437-2.00003-X.